Active matter invasion of a viscous fluid: Unstable sheets and a no-flow theorem

Christopher J. Miles*
Department of Physics, University of Michigan, 450 Church St., Ann Arbor, Michigan 48109, USA

Arthur A. Evans
Department of Mathematics, University of Wisconsin-Madison, 480 Lincoln Dr., Madison, Wisconsin 53706, USA

Michael J. Shelley
Flatiron Institute, Simons Foundation, New York, New York, USA;
and Courant Institute of Mathematical Sciences, New York University, New York, New York 10012, USA

Saverio E. Spagnolie†
Department of Mathematics, University of Wisconsin-Madison, 480 Lincoln Dr., Madison, Wisconsin 53706, USA

(Received 14 March 2018; revised manuscript received 29 November 2018; published 4 March 2019)

We investigate the dynamics of a dilute suspension of hydrodynamically interacting motile or immotile stress-generating swimmers or particles as they invade a surrounding viscous fluid. Colonies of aligned pusher particles are shown to elongate in the direction of particle orientation and undergo a cascade of transverse concentration instabilities, governed at small times by an equation that also describes the Saffman-Taylor instability in a Hele-Shaw cell, or the Rayleigh-Taylor instability in a two-dimensional flow through a porous medium. Thin sheets of aligned pusher particles are always unstable, while sheets of aligned puller particles can either be stable (immotile particles), or unstable (motile particles) with a growth rate that is nonmonotonic in the force dipole strength. We also prove a surprising "no-flow theorem": a distribution initially isotropic in orientation loses isotropy immediately but in such a way that results in no fluid flow *everywhere and for all time*.

DOI: 10.1103/PhysRevLett.122.098002

The last decade has seen an explosion of interest in the collective dynamics of active particles immersed in fluids, from swimming microorganisms to magnetically driven and phoretic colloidal particles [1–13] to kinesin-driven microtubule assemblies [14–21]. A first-principles model of active suspensions is a mean-field kinetic theory that tracks the distribution of particle positions and orientations and which may include hydrodynamic interactions [7,10,22–24] and short-range physics [24,25]. Constituent particles are classified as either "pushers" or "pullers" depending on the sign of the generated stresslet flow, which in turn depends on the geometry of the body and the mechanism of stress generation [23,26–30]. Other models include Landau-de Gennes "Q tensor" theories and moment-closure theories [31–36]. Generic features in these systems include long-range coherence, topological defects, and instability [23,36–41].

Much is known about active suspensions that cover the entire available physical domain. Far less is known about the invasion of a surrounding particle-free environment, though this is of considerable importance in the dynamic self-assembly of swarms [42–44], and in the formation of biofilms, mycelia, and fruiting bodies [45,46]. Novel means of bringing bacteria into a confined region using external flows have allowed for a closer look at rapid expansion, including acoustic trapping [47,48], UV light exposure [49], and vortical flows [50,51]. The effects of confinement by soft boundaries with surface tension has seen theoretical treatment [52,53], and unstable bands of active particles have been studied in a dry system [54].

In this Letter, we investigate the dynamics of colonies of either motile or immotile active particles as they invade a surrounding viscous fluid. Colonies of aligned pushers are shown to elongate in the direction of particle orientation and then undergo a cascade of transverse concentration instabilities. The initial instability in two-dimensions is shown to be governed at small times by an equation that also describes the Saffman-Taylor instability in a Hele-Shaw cell (flow through a small gap between two nearby plates), or the Rayleigh-Taylor instability in a two-dimensional flow through a porous medium. Linear stability analysis offers approximations that match the results of full numerical simulations. We close with a proof and demonstration of a counter-intuitive "no-flow theorem," that an isotropically oriented distribution with any initial concentration profile results in no fluid flow everywhere and for all time.

Mathematical model.—Following Refs. [23,24], we describe a dilute suspension of N self-propelled rodlike particles in a viscous fluid by the particle distribution function, $\Psi(\mathbf{x}, \mathbf{p}, t)$, where $\mathbf{x}$ is the particle position in a

periodic spatial domain D while $\mathbf{p}$ is the particle orientation vector on the unit ball S ($|\mathbf{p}| = 1$). The number of particles is conserved, $N = \int_D \int_S \Psi(\mathbf{x}, \mathbf{p}, t) d\mathbf{p} d\mathbf{x}$, resulting in a Smoluchowski equation,

$$\Psi_t + \nabla \cdot (\dot{\mathbf{x}}\Psi) + \nabla_{\mathbf{p}} \cdot (\dot{\mathbf{p}}\Psi) = 0, \tag{1}$$

where $\nabla = \nabla_{\mathbf{x}} = \partial/\partial\mathbf{x}$ and $\nabla_{\mathbf{p}} = (\mathbf{I} - \mathbf{pp}) \cdot \partial/\partial\mathbf{p}$. Neglecting collisions [40], the fluxes $\dot{\mathbf{x}}$ and $\dot{\mathbf{p}}$ are given by

$$\dot{\mathbf{x}} = V_0\mathbf{p} + \mathbf{u}(\mathbf{x}) - d_t\nabla(\ln\Psi), \tag{2}$$

$$\dot{\mathbf{p}} = (\mathbf{I} - \mathbf{pp}) \cdot (\mathbf{p} \cdot \nabla\mathbf{u}) - d_r\nabla_{\mathbf{p}}(\ln\Psi), \tag{3}$$

with V_0 the swimming speed, d_t (d_r) the translational (rotational) diffusivity, $\mathbf{u}(\mathbf{x}, t)$ the fluid velocity, and $\mathbf{pp}$ a dyadic product.

The environment is assumed to be a viscous Newtonian fluid, driven by stresses generated by the suspended particles. The flow field $\mathbf{u}$ satisfies the Stokes equations, consisting of momentum and mass conservation,

$$-\nabla q + \mu\nabla^2\mathbf{u} + \nabla \cdot \boldsymbol{\Sigma}_a = \mathbf{0}, \qquad \nabla \cdot \mathbf{u} = 0, \tag{4}$$

with q the pressure, μ the dynamic viscosity, and $\boldsymbol{\Sigma}_a = \sigma\langle\mathbf{pp}\rangle$ the active stress (proportional to the second orientational moment of Ψ, see below). The coefficient σ is the force dipole (or stresslet) strength, with $\sigma < 0$ for pushers and $\sigma > 0$ for pullers [10], which has been computed for ellipsoidal Janus particles [27,29] and for more general particle types [30,55,56], and obtained experimentally for a few swimming cells [57,58]. Orientational moments will be denoted by $\langle h(\mathbf{p})\rangle = \int_S h(\mathbf{p})\Psi d\mathbf{p}$. For example, integrating Eq. (1) gives an evolution equation for the particle concentration, $c = \langle 1\rangle$, namely,

$$c_t + \nabla \cdot (c\mathbf{u}) - d_t\nabla^2 c = -V_0\nabla \cdot \langle\mathbf{p}\rangle, \tag{5}$$

where $\langle\mathbf{p}\rangle$ is the polarity [10].

With ℓ the individual particle length, we scale velocities by the swimming speed V_0 and lengths by the mean free path $\ell_c = (V/V_p)\ell$, where V is the total fluid volume and $V_p = N\ell^3$ is an effective volume of particles, hence $\ell_c = V(N\ell^2)^{-1}$. Time is scaled by ℓ_c/V_0, force densities are scaled by $\mu V_0/\ell_c^2$, and Ψ is normalized by the particle number density, $N/V = (\ell^2\ell_c)^{-1} = (\ell/\ell_c)\ell^{-3}$. The dimensionless dipole strength is defined as $\alpha = \sigma/[\mu V_0\ell_c^2]$. With all variables now taken to be dimensionless, particle conservation is written as $\tilde{\kappa}^{-1}\int_D\int_S \Psi d\mathbf{p} d\mathbf{x} = 1$, where $\tilde{\kappa}^{-1} = \ell_c^3/V$ is proportional to the particle volume fraction. In the case of immotile particles, a different velocity scale must be chosen [59].

The far-field velocity due to an individual swimmer at the origin, oriented in the direction $\mathbf{p}$, is $\mathbf{u} = \alpha(8\pi)^{-1}\mathbf{pp} : \nabla\mathbf{G}(\mathbf{x})$ where $G_{ij} = \delta_{ij}/|\mathbf{x}| + x_i x_j/|\mathbf{x}|^3$ is the Stokeslet singularity [60]. The active force density is then given by $\mathbf{f}_a = \alpha(\ell_c/\ell)^2\nabla \cdot \langle\mathbf{pp}\rangle$. Following Ref. [23], for the sake of comparison, we set $\ell_c/\ell = 1$. The swimming speed V_0, now taken as dimensionless, is unity for motile systems and zero otherwise.

We will consider the case of confinement to motion in two-dimensions in a periodic domain $(x, y) \in [0, L) \times [0, H)$, and invariance in the $\hat{\mathbf{z}}$ direction, writing $\mathbf{p} = (\cos\theta, \sin\theta, 0)$ and the distribution as $\Psi(x, y, \theta, t)$. It is expedient to then define $\kappa = HL$ so that $\kappa^{-1}\int_0^L\int_0^H\int_0^{2\pi}\Psi d\theta dy dx = 1$. Numerical solution of Eqs. (1)–(4) is carried out using $L = H = 50$ and a pseudospectral method with 256^3 grid points and dealiasing (using the 3/2 rule) [61]; an integrating factor method, along with a second-order accurate Adams-Bashforth scheme, is used for time stepping.

Dynamics of thin active sheets.—To motivate the study to come we first consider the invasion of a concentrated cylindrical colony, Gaussian in cross section, of motile particles initially aligned in the $\hat{\mathbf{x}}$ direction into an empty viscous fluid, shown in Fig. 1(a). The associated global flow field is exactly that of a single regularized force dipole, resulting for pullers in a stable concentration elongation in a direction orthogonal to the original swimmer orientation [59,62]. For pushers, the colony-induced velocity field changes sign and elongation is parallel to the swimming direction, but if slightly perturbed a transverse concentration instability ensues. Fore-aft symmetry is broken due to particle motility; the colony splays at the leading tip on the right, while undergoing a periodic folding at the rear, reminiscent of the buckling of planar viscous jets, sedimenting elastic filaments, and beams extruded into viscous fluids [63–65].

To better understand this dramatic evolution, we turn to the behavior of an infinite sheet of particles that are initially in alignment. Figure 1(b) shows the evolution of a distribution of immotile (top) and motile (bottom) pusher particles, initially confined to a thin band, and with a small transverse concentration perturbation. Early stages show rapid growth of the wave amplitude. At the same time, individual particles are rotated so that they remain nearly tangent to the concentration band which results in a secondary instability and self-folding. The same structures are observed again and again on smaller length scales, though particle motility breaks left-right symmetry and significantly alters the structure of subsequent folding events. At longer times, the system is finally drawn to an unsteady roiling state (see Ref. [59]), with uniform concentration for immotile particles [c satisfies a pure advection-diffusion equation in Eq. (5) in this case] or concentration bands described by Saintillan and Shelley [23] for motile particles.

To analyze the instability, let $h(x, t)$ and $\phi(x, t)$ represent the vertical displacement and polarity of the line distribution, respectively, with $\mathbf{n} = \langle\mathbf{p}\rangle/c = (\cos\phi, \sin\phi, 0)$ the normalized polarity. We study the dynamics of this active

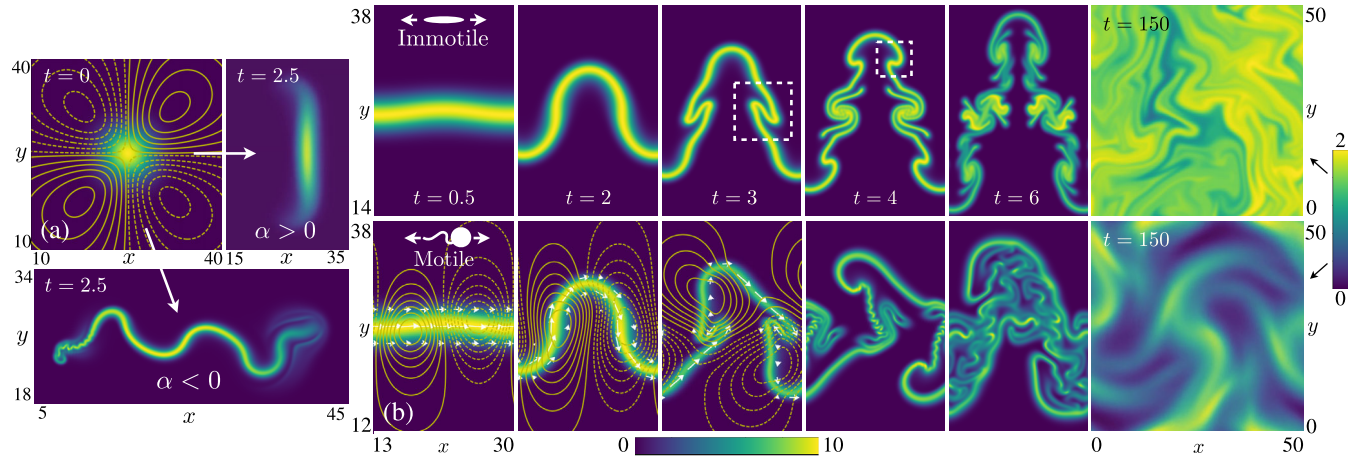

FIG. 1. (a) Concentration evolution of a weakly perturbed cylindrical colony (Gaussian in cross section) of aligned motile pullers ($\alpha = 0.5$, right) and pushers ($\alpha = -0.5$, bottom). Stream function contours are included at $t = 0$ with solid (dashed) lines representing positive (negative) values if $\alpha < 0$, and the signs are reversed if $\alpha > 0$. See Supplemental Material Movie M1 [59]. (b) Evolution of a thin sheet of immotile (top) and motile (bottom) pusher particles with $\alpha = -1$, with initial distribution function $\Psi(\mathbf{x}, \theta, t = 0) = C \exp\{-(y - h(x))^2/a^2 - \theta^2/b^2\}$ and C a normalization constant. The initial perturbation is given by $h(x) = 0.1 \sin(6\pi x/L)$ and $(a, b) = (2, 0.2)$. The polarity field $\langle \mathbf{p} \rangle$ (arrows) shows the local particle orientation. Exponential growth in amplitude leads to a secondary instability and self-folding at $t \approx 2.5$, which plays out again at $t \approx 4$ with similar features on a smaller scale (dashed boxes). The small initial spread in orientation and small noise results in eventual loss of symmetry and the system arrives in an unsteady roiling state ($t = 150$) with uniform concentration (immotile particles) or concentration bands (motile particles). See Supplemental Material Movie M2 [59].

sheet via its far-field self-influence. For small h and ϕ, and solving Eq. (4) for $\mathbf{u}$ [59], we find

$$h_t + V_0 h_x = v + V_0 \phi, \qquad \phi_t + V_0 \phi_x = v_x, \tag{6}$$

$$v = -\frac{\alpha\kappa}{4L} \mathcal{H}[h_x], \tag{7}$$

where v is the vertical component of velocity evaluated on the flat surface $h = 0$, and $\mathcal{H}[\cdot]$ is the Hilbert transform,

$$\mathcal{H}[f](x) = \frac{1}{\pi} \mathrm{P} \int_{-\infty}^{\infty} \frac{f(y)}{x - y} dy, \tag{8}$$

where P denotes principal value. The Hilbert transform is diagonalized in a Fourier basis, with $\mathcal{H}[e^{iqx}] = -i\,\mathrm{sign}(q) e^{iqx}$. The ansatz $\langle h(x,t), \phi(x,t) \rangle = \sum_k \langle \hat{h}_k(t), \hat{\phi}_k(t) \rangle \exp(2\pi i k x/L)$ therefore results in a quadratic eigenvalue problem, and the eigenvalues

$$\lambda_\pm = \frac{\pi}{4L^4} (-\alpha\kappa|k| - 8ikLV_0 \pm \gamma_k), \tag{9}$$

where $\gamma_k = \sqrt{\alpha\kappa(\alpha\kappa k^2 - 16iLV_0 k|k|)}$. A comparison to numerics is shown in Fig. 2 for motile pushers with three negative dipole strengths along with the theory for a wider range of α and k. The analytical predictions are accurate for the entire range studied, with discrepancies owing to the vertical periodic boundary condition and the nonvanishing thickness of the active sheet in the simulations.

In the immotile case, $V_0 = 0$ (or in the limit as $|\alpha|/V_0 \to \infty$), sheets of pushers are all unstable and sheets of pullers are all stable, with growth and decay rates both given by $-\pi\alpha\kappa|k|/(2L^2)$. This behavior owes to the velocity field created by the active stress, illustrated in Fig. 2 (see Supplemental Material Movie M2 [59]), which amplifies or damps the initial perturbation. The linearized dynamics are now governed solely by the equation

$$h_t = \frac{-\alpha\kappa}{4L} \mathcal{H}[h_x]. \tag{10}$$

This expression establishes an unexpected connection to well-studied phenomena in entirely different settings:

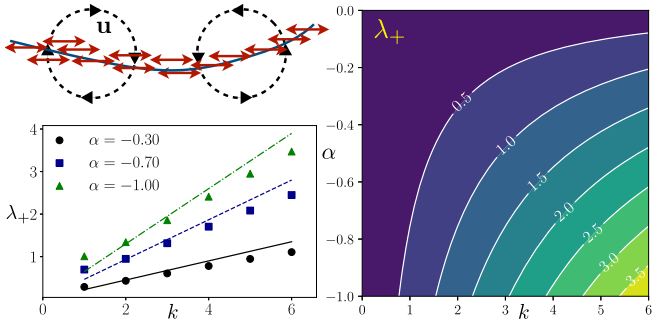

FIG. 2. (Top left) A sheet of aligned pushers is unstable to transverse concentration perturbations due to its self-generated velocity field. (Bottom left) The positive growth rate for motile pushers, comparing numerics and theory. (Right) Theoretical growth rates for motile pushers for a range of dipole strengths and wave numbers.

interfacial instabilities in gravity or pressure-driven Hele-Shaw problems, or two-dimensional flows in porous media, without surface tension, whose flow is governed by Darcy's Law [66,67] (also known as the Muskat problem [68,69]). As in the present setting, the classical Rayleigh-Taylor instability is modified to an exponential growth rate dependence which is linear in $|k|$ [70]. Such interfacial instabilities are associated with the formation of singularities in free-surface flows, e.g., the finite-time "Moore singularity" development on a vortex sheet in an inviscid fluid with no surface tension described by the Kelvin-Helmholtz instability [71,72], a higher-order system that shares linear growth rate dependence on $|k|$ [73–77]. We thus observe an identical initial growth behavior, but nonlinear terms for large amplitude waves result in a unique folding event in $t \approx 2.5$ in Fig. 1(b) and very different long-time behavior.

Meanwhile in the motile case, $V_0 = 1$, sheets of pushers remain unstable for any dipole strength. Sheets of pullers, however, excite a positive-real-part eigenvalue in Eq. (9). Unlike in the case of pushers, the maximal eigenvalue is not monotonic in the force dipole strength (Fig. 3). Expanding about small α, the largest eigenvalue is found when $\alpha = 2L/\kappa$, at which point $\mathrm{Re}[\lambda_+] = \pi k(2L)^{-1}$ (since $\mathrm{Re}[\lambda_+] \sim \pi k\alpha\kappa(4L^2)^{-1}$). For either motile or immotile pullers, the velocity field (oppositely signed to that illustrated in Fig. 2) rapidly damps the initial displacement, and it now rotates particles towards the direction *perpendicular* to the concentration band. Motility, however, allows the displacement and orientation fields to synchronize, leading ultimately to the rapid growth of the concentration band amplitude and a large departure away from the initial profile, as shown in Fig. 3.

For the motile suspensions above with nonzero dipole strength α, there can be competing effects; in particular, if $\max(\mathrm{Re}[\lambda_\pm]) < 0$, all solutions to the linear system eventually arrive at the stable base state, but if the system

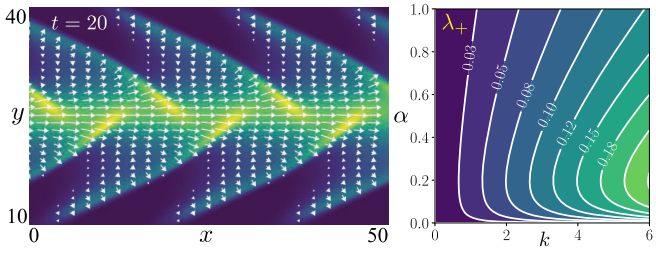

FIG. 3. (Left) Sheets of motile puller particles are unstable (here $\alpha = 0.1$ and $d_t = d_r = 0.001$). Arrows show the polarity field, $\langle \mathbf{p} \rangle$, at $t = 20$. See Supplemental Material Movie M3 [59]. The initial condition is along an unstable eigenvector, $h(x,0) = 0.144\cos(6\pi x/L) - 0.063\sin(6\pi x/L)$ and $\phi(x,0) = 0.1\cos(6\pi x/L)$. (Right) Theoretical growth rates for motile pullers are nonmonotonic in α.

departs from the linearized region of the phase space fast enough such solutions may not be realized in the fully nonlinear dynamics. This potential for departure is seen most clearly if the particles are not stress generating: with $\alpha = 0$, the wave amplitude grows linearly in time since any particles with a nonzero initial orientation angle drift off without resistance along characteristic curves.

Isotropic suspensions remain velocity free: a "no-flow theorem": Assuming the uniqueness of solutions to Eqs. (1)–(4), active suspensions of motile or immotile particles modeled by Eqs. (1)–(4), which are initially isotropic in orientation, $\Psi(\mathbf{x}, \mathbf{p}, t = 0) = \Psi_0(\mathbf{x})$, result in no fluid flow, $\mathbf{u}(\mathbf{x}, t) = \mathbf{0}$, *everywhere and for all time*.

Sketch of the proof.—The proof assumes the uniqueness of solutions to Eqs. (1)–(4), which was shown for two dimensions by Chen and Liu [78]. Consider first the solution Ψ^* to the Smoluchowski equation without velocity terms,

$$\Psi^*_t + V_0\mathbf{p}\cdot\nabla\Psi^* - d_t\nabla^2_{\mathbf{x}}\Psi^* - d_r\nabla^2_{\mathbf{p}}\Psi^* = 0, \quad (11)$$

with an initial condition that is isotropic in orientation. The velocity field generated by this solution, $\mathbf{u}[\Psi^*]$, is given in Fourier space by

$$\hat{\mathbf{u}}_{\mathbf{k}}[\Psi^*] = (8\pi|\mathbf{k}|^2)^{-1}(\mathbf{I} - \hat{\mathbf{k}}\hat{\mathbf{k}})\cdot\hat{\boldsymbol{\Sigma}}_a\cdot\mathbf{k}, \quad (12)$$

$$\hat{\boldsymbol{\Sigma}}_a\cdot\mathbf{k} = \int_D \mathbf{p}(\mathbf{p}\cdot\mathbf{k})\hat{\Psi}^*_{\mathbf{k}}(\mathbf{p},t)d\mathbf{p}, \quad (13)$$

where $\hat{\mathbf{k}} = \mathbf{k}/|\mathbf{k}|$. Writing $\mathbf{k}$ in a spherical (three-dimensional) or polar (two-dimensional) coordinate system about $\mathbf{p}$, we find $\hat{\boldsymbol{\Sigma}}_a\cdot\mathbf{k} = \lambda_{\mathbf{k}}(t)\mathbf{k}$ for some scalar function $\lambda_{\mathbf{k}}(t)$. Hence, $\hat{\mathbf{u}}_{\mathbf{k}}[\Psi^*] = \mathbf{0}$ and then $\mathbf{u}[\Psi^*] = \mathbf{0}$. Since $\mathbf{u}[\Psi^*] = \mathbf{0}$, Ψ^* also solves Eqs. (1)–(4) with velocity terms included. By the uniqueness assumption, we finally have that $\mathbf{u} = \mathbf{0}$ everywhere and for all time for any initially isotropic distribution. More details are included in the Supplemental Material [59].

The result is surprising since the system immediately loses orientational isotropy (see Fig. 4), which would suggest the quick onset of a nontrivial flow field, but this is not what we observe. Physically, the active force $\mathbf{f}_a = \nabla\cdot\boldsymbol{\Sigma}_a$ is nontrivial for any $t > 0$ but it is curl-free, so by the Helmholtz decomposition theorem, $\mathbf{f}_a = \nabla\lambda(t)$ for some scalar field $\lambda(t)$, which thus only modifies the pressure. As time progresses, the force distribution evolves with the local active particle alignment, illustrated for two initially uniform colonies in Fig. 4, but the expanding colonies simply pass through each other as linear waves. This behavior can be inferred even when including two-particle correlations [79].

Moreover, any distributions that result in $\mathbf{u} = \mathbf{0}$ for all time may be superimposed without generating a velocity field, for instance a random isotropic distribution may be

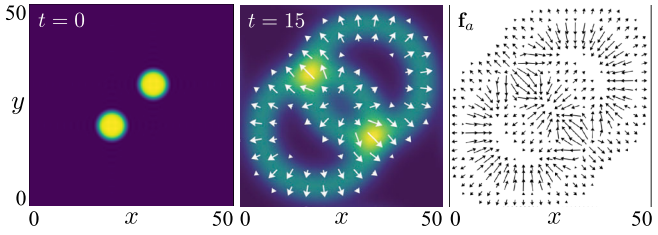

FIG. 4. The no-flow theorem playing out in a simple setting. Two circular isotropically oriented colonies expand radially and pass through each other without interacting. The polarity field $\langle \mathbf{p} \rangle$ at $t = 15$ shows local alignment. The active force $\mathbf{f}_a = \nabla \cdot \mathbf{\Sigma}_a$ (right, at $t = 15$) is curl-free, modifying only the pressure and resulting in no fluid flow, $\mathbf{u} = \mathbf{0}$ for all time. This linear superposition generalizes to arbitrary initial concentration fields. See Supplemental Material Movie M4 [59].

perturbed by another distribution which has the property that $\nabla \cdot \langle \mathbf{pp} \rangle = \nabla \chi(t)$ for any scalar $\chi(t)$, and still $\mathbf{u} = \mathbf{0}$ for all time. Physics that introduce nonlinearities in Eq. (1), such as near-field steric repulsion, are expected to nullify the theorem.

The stability of the theorem to an initial localized alignment is not simply determined, as the initially isotropic state is not a stable base state. However, in light of the stability of the isotropic state of uniform concentration to large wave number perturbations [23], we expect an initial damping back towards isotropy. But on an extremely long timescale in a sufficiently large domain, the low wave number residue of the initial disruption is expected to lead to eventual growth along with a nontrivial flow. We have verified this prediction in at least one setting by numerical simulation, placing an aligned colony, as in Fig. 1(a), into a random concentration field that is orientationally isotropic. Persistent nematic alignment, for instance, due to a boundary, may result in a more immediate transition to a global mean flow.

Conclusion.—We have investigated colonies of active particles in the dilute regime invading a quiescent fluid. Colony-scale elongation depends on the sign of the active stress and can result in a self-buckling and self-folding cascade. Exponential growth at small times, with growth rate linear in $|k|$, is mathematically equivalent to the Saffman-Taylor instability in a Hele-Shaw cell or Rayleigh-Taylor instability in a two-dimensional flow through a porous medium. The stability of sheets of pullers depends on particle motility with a growth rate that is nonmonotonic in the dipole strength. Strikingly, a suspension modeled by pure far-field hydrodynamic interactions which is initially isotropic in orientation, even though isotropy is not preserved, results in no mean-field fluid flow everywhere and for all time.

This project was initiated at the Woods Hole Oceanographic Institute as part of the Geophysical Fluid Dynamics summer program. Financial support is acknowledged by M. J. S. (National Science Foundation Grants No. DMR-0820341 [NYU MRSEC], No. DMS-1463962, and No. DMS-1620331) and S. E. S. (Grants No. DMR 767-1121288 [UW MRSEC] and No. DMS-1661900).

*cmiless@umich.edu
†spagnolie@math.wisc.edu

[1] T. J. Pedley and J. O. Kessler, Annu. Rev. Fluid Mech. **24**, 313 (1992).
[2] C. Dombrowski, L. Cisneros, S. Chatkaew, R. E. Goldstein, and J. O. Kessler, Phys. Rev. Lett. **93**, 098103 (2004).
[3] L. H. Cisneros, R. Cortez, C. Dombrowski, R. E. Goldstein, and J. O. Kessler, Exp. Fluids **43**, 737 (2007).
[4] P. T. Underhill, J. P. Hernandez-Ortiz, and M. D. Graham, Phys. Rev. Lett. **100**, 248101 (2008).
[5] A. Baskaran and M. M. Cristina, Proc. Natl. Acad. Sci. U.S.A. **106**, 15567 (2009).
[6] S. Ramaswamy, Annu. Rev. Condens. Matter Phys. **1**, 323 (2010).
[7] D. L. Koch and G. Subramanian, Annu. Rev. Fluid Mech. **43**, 637 (2011).
[8] T. Vicsek and A. Zafeiris, Phys. Rep. **517**, 71 (2012).
[9] M. C. Marchetti, J. F. Joanny, S. Ramaswamy, T. B. Liverpool, J. Prost, M. Rao, and R. A. Simha, Rev. Mod. Phys. **85**, 1143 (2013).
[10] D. Saintillan and M. J. Shelley, in *Complex Fluids in Biological Systems* (Springer, New York, 2015), pp. 319–351.
[11] J. Elgeti, R. G. Winkler, and G. Gompper, Rep. Prog. Phys. **78**, 056601 (2015).
[12] A. Zöttl and H. Stark, J. Phys. Condens. Matter **28**, 253001 (2016).
[13] K. Yeo, E. Lushi, and P. M. Vlahovska, Soft Matter **12**, 5645 (2016).
[14] K. J. Helmke, R. Heald, and J. D. Wilbur, Int. Rev. Cell Mol. Biol. **306**, 83 (2013).
[15] T. Sanchez, D. T. N. Chen, S. J. DeCamp, M. Heymann, and Z. Dogic, Nature (London) **491**, 431 (2012).
[16] F. C. Keber, E. Loiseau, T. Sanchez, S. J. DeCamp, L. Giomi, M. J. Bowick, M. C. Marchetti, A. Dogic, and A. R. Bausch, Science **345**, 1135 (2014).
[17] J. Prost, F. Jülicher, and J.-F. Joanny, Nat. Phys. **11**, 111 (2015).
[18] P. J. Foster, S. Fürthauer, M. J. Shelley, and D. J. Needleman, eLife **4**, e10837 (2015).
[19] T. Gao, R. Blackwell, M. A. Glaser, M. D. Betterton, and M. J. Shelley, Phys. Rev. Lett. **114**, 048101 (2015).
[20] M. J. Shelley, Annu. Rev. Fluid Mech. **48**, 487 (2016).
[21] I. Maryshev, D. Marenduzzo, A. B. Goryachev, and A. Morozov, Phys. Rev. E **97**, 022412 (2018).
[22] D. Saintillan and M. J. Shelley, Phys. Rev. Lett. **99**, 058102 (2007).
[23] D. Saintillan and M. J. Shelley, Phys. Fluids **20**, 123304 (2008).
[24] G. Subramanian and D. L. Koch, J. Fluid Mech. **632**, 359 (2009).
[25] V. Mehandia and P. R. Nott, J. Fluid Mech. **595**, 239 (2008).
[26] E. Lauga and T. Powers, Rep. Prog. Phys. **72**, 096601 (2009).

[27] S. E. Spagnolie and E. Lauga, J. Fluid Mech. **700**, 105 (2012).
[28] S. Ghose and R. Adhikari, Phys. Rev. Lett. **112**, 118102 (2014).
[29] E. Lauga and S. Michelin, Phys. Rev. Lett. **117**, 148001 (2016).
[30] B. Nasouri and G. J. Elfring, Phys. Rev. Fluids **3**, 044101 (2018).
[31] S. Ramaswamy, R. A. Simha, and J. Toner, Eur. Phys. Lett. **62**, 196 (2003).
[32] F. G. Woodhouse and R. E. Goldstein, Phys. Rev. Lett. **109**, 168105 (2012).
[33] M. G. Forest, Q. Wang, and R. Zhou, Soft Matter **9**, 5207 (2013).
[34] L. Giomi, M. J. Bowick, X. Ma, and M. C. Marchetti, Phys. Rev. Lett. **110**, 228101 (2013).
[35] S. P. Thampi, R. Golestanian, and J. M. Yeomans, Phys. Rev. Lett. **111**, 118101 (2013).
[36] T. Brotto, J.-B. Caussin, E. Lauga, and D. Bartolo, Phys. Rev. Lett. **110**, 038101 (2013).
[37] R. A. Simha and S. Ramaswamy, Phys. Rev. Lett. **89**, 058101 (2002).
[38] C. Hohenegger and M. J. Shelley, Phys. Rev. E **81**, 046311 (2010).
[39] E. Bertin, H. Chaté, F. Ginelli, S. Mishra, A. Peshkov, and S. Ramaswamy, New J. Phys. **15**, 085032 (2013).
[40] B. Ezhilan, M. J. Shelley, and D. Saintillan, Phys. Fluids **25**, 070607 (2013).
[41] X. Shi, H. Chaté, and Y. Ma, New J. Phys. **16**, 035003 (2014).
[42] J. A. Shapiro, M. Dworkin *et al.*, *Bacteria as Multicellular Organisms* (Oxford University Press, Oxford, 1997).
[43] M. F. Copeland and D. B. Weibel, Soft Matter **5**, 1174 (2009).
[44] N. C. Darnton, L. Turner, S. Rojevsky, and H. C. Berg, Biophys. J. **98**, 2082 (2010).
[45] D. Claessen, D. E. Rozen, O. P. Kuipers, L. Søgaard-Andersen, and G. P. Van Wezel, Nat. Rev. Microbiol. **12**, 115 (2014).
[46] Y. I. Yaman, E. Demir, R. Vetter, and A. Kocabas, arXiv: 1811.12076.
[47] S. C. Takatori, R. De Dier, J. Vermant, and J. F. Brady, Nat. Commun. **7**, 10694 (2016).
[48] S. Gutiérrez-Ramos, M. Hoyos, and J. C. Ruiz-Suárez, Sci. Rep. **8**, 4668 (2018).
[49] A. E. Patteson, A. Gopinath, and P. E. Arratia, arXiv: 1805.06429.
[50] A. Sokolov and I. S. Aranson, Nat. Commun. **7**, 11114 (2016).
[51] A. Sokolov, L. D. Rubio, J. F. Brady, and I. S. Aranson, Nat. Commun. **9**, 1322 (2018).
[52] T. Gao and Z. Li, Phys. Rev. Lett. **119**, 108002 (2017).
[53] T. Gao, M. D. Betterton, A.-S. Jhang, and M. J. Shelley, Phys. Rev. Fluids **2**, 093302 (2017).
[54] S. Ngo, A. Peshkov, I. S. Aranson, E. Bertin, F. Ginelli, and H. Chaté, Phys. Rev. Lett. **113**, 038302 (2014).
[55] O. S. Pak and E. Lauga, in *Fluid–Structure Interactions in Low-Reynolds-Number Flows* (Royal Society of Chemistry, London, 2015), pp. 100–167.
[56] H. Reinken, S. H. L. Klapp, M. Bär, and S. Heidenreich, Phys. Rev. E **97**, 022613 (2018).
[57] K. Drescher, R. E. Goldstein, N. Michel, M. Polin, and I. Tuval, Phys. Rev. Lett. **105**, 168101 (2010).
[58] K. Drescher, J. Dunkel, L. Cisneros, S. Ganguly, and R. E. Goldstein, Proc. Natl. Acad. Sci. U.S.A. **108**, 10940 (2011).
[59] See Supplemental Material at http://link.aps.org/supplemental/10.1103/PhysRevLett.122.098002 for more detailed calculations.
[60] C. Pozrikidis, *Boundary Integral and Singularity Methods for Linearized Viscous Flow* (Cambridge University Press, Cambridge, England, 1992).
[61] B. Fornberg, *A Practical Guide to Pseudospectral Methods*, Vol. 1 (Cambridge University Press, Cambridge, England, 1998).
[62] R. Cortez, SIAM J. Sci. Comput. **23**, 1204 (2001).
[63] J. Cruickshank and B. R. Munson, J. Fluid Mech. **113**, 221 (1981).
[64] L. Li, H. Manikantan, D. Saintillan, and S. E. Spagnolie, J. Fluid Mech. **735**, 705 (2013).
[65] F. P. Gosselin, P. Neetzow, and M. Paak, Phys. Rev. E **90**, 052718 (2014).
[66] G. Tryggvason and H. Aref, J. Fluid Mech. **136**, 1 (1983).
[67] T. Y. Hou, J. S. Lowengrub, and M. J. Shelley, J. Comput. Phys. **114**, 312 (1994).
[68] M. Siegel, R. E. Caflisch, and S. Howison, Commun. Pure Appl. Math. A **57**, 1374 (2004).
[69] A. Córdoba, D. Córdoba, and F. Gancedo, Ann. Math. **173**, 477 (2011).
[70] P. G. Saffman and G. I. Taylor, Proc. R. Soc. A **245**, 312 (1958).
[71] G. Birkhoff, in Proc. Symp. Appl. Math. **13**, 55 (1962).
[72] F. Charru, *Hydrodynamic Instabilities* (Cambridge University Press, Cambridge, England, 2011).
[73] D. W. Moore, Proc. R. Soc. A **365**, 105 (1979).
[74] D. I. Meiron, G. R. Baker, and S. A. Orszag, J. Fluid Mech. **114**, 283 (1982).
[75] R. Krasny, J. Fluid Mech. **167**, 65 (1986).
[76] M. J. Shelley, J. Fluid Mech. **244**, 493 (1992).
[77] S. J. Cowley, G. R. Baker, and S. Tanveer, J. Fluid Mech. **378**, 233 (1999).
[78] X. Chen and J.-G. Liu, J. Differ. Equations **254**, 2764 (2013).
[79] J. Stenhammar, C. Nardini, R. W. Nash, D. Marenduzzo, and A. Morozov, Phys. Rev. Lett. **119**, 028005 (2017).

Active matter invasion of a viscous fluid: Unstable sheets and a no-flow theorem - Supplemental material

A. Flow due to a single active particle

The flow generated by a single active particle, for instance a swimming *E. coli* cell (Fig. 1a), can result in a coherent organization of many such particles on much longer length scales than the individual particle size (exhibited by a suspension of *B. subtilis* cells in Fig. 1b).

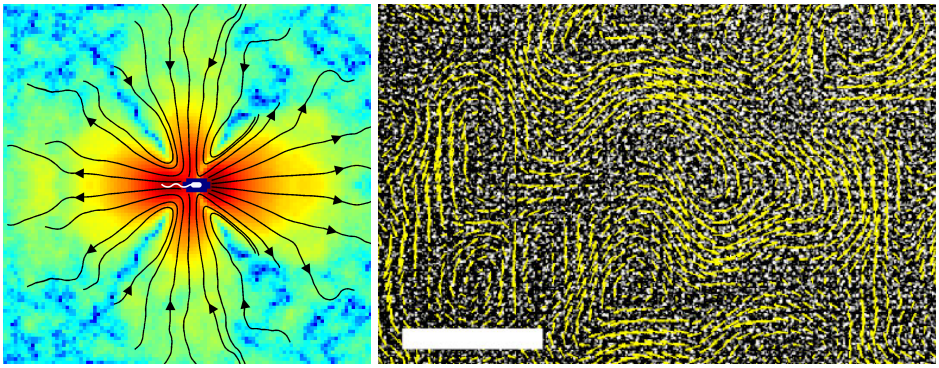

FIG. 1. Left: Experimental particle-image-velocity (PIV) near an *E. coli* cell ([1], with permission). Right: A swimming suspension of *B. subtilis* cells ([2], with permission), overlaid with a PIV flow field. The scale bar is 35 μm; the longest arrows correspond to a velocity of 30 $\mu m/s$.

We begin by providing a very simple model to clarify the relationship of the parameter σ in the mean-field model to the force dipole strength of an individual organism. A single force/torque-free swimming body, as illustrated in Fig. 2a, may be viewed as a moving hydrodynamic force dipole in the far-field, where the force on the fluid from the flagellum is balanced by that on the moving cell body. In the simple model shown in Fig. 2b the cell body is treated as a sphere of radius A, and the flagellum is idealized as a small sphere of radius a a distance d from the cell body and moving with speed $v - V_0$ along the $-\hat{\mathbf{x}}$ axis (i.e. with relative speed v away from the cell body).

In the simplest theory hydrodynamic interactions are neglected beyond demanding force balance. The forces on the fluid due to the cell body and "flagellum" are given by the leading order Faxén's law (neglecting terms of order d^{-1} and beyond), $F_A = 6\pi\mu A V_0$ and $F_a = 6\pi\mu a(V_0 - v)$, respectively. With no external force acting on the body we must have $F_A + F_a = 0$, which results in the swimming speed $V_0 = av/(A + a)$. Placing the cell body at the origin, the flow far away from the cell is given by:

$$\mathbf{u} \approx \frac{1}{8\pi\mu}\left[\mathbf{G}_{(3)}(\mathbf{x}) - \mathbf{G}_{(3)}(\mathbf{x} - d\hat{\mathbf{x}})\right] \cdot (F_A\hat{\mathbf{x}}), \tag{1}$$

where $\hat{\mathbf{x}} = \mathbf{x}/|\mathbf{x}|$, $\mathbf{xx}$ is a dyadic product, and

$$\mathbf{G}_{(3)}(\mathbf{x}) = \frac{1}{|\mathbf{x}|}\left(\mathbf{I} + \frac{\mathbf{xx}}{|\mathbf{x}|^2}\right) \tag{2}$$

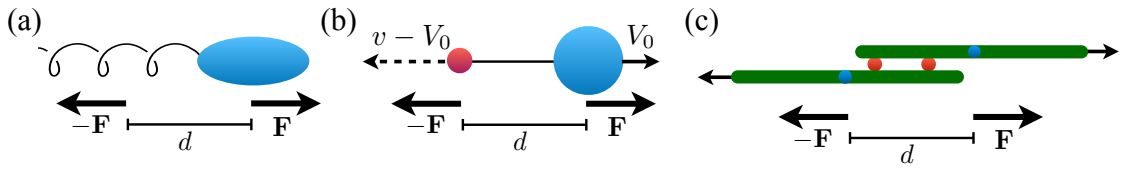

FIG. 2. (a) A neutrally-buoyant swimming organism is a hydrodynamic force dipole in the far-field, with fluid forcing from the flagellum and the moving cell in balance. (b) A simplified swimming model, where the flagellum is treated as a sphere a distance d from the cell body which moves with speed $v - V_0$ to the left. Through force balance this drives the cell body to move to the right with the "swimming speed" V_0. (c) Biofilaments sliding past each other by the action of molecular motors can also be viewed as imposing a force dipole on the surrounding fluid.

is the Stokeslet singularity in three-dimensions [3]. For large $|\mathbf{x}|$ we expand to find

$$\mathbf{u} \approx \frac{dF_A}{8\pi\mu}\hat{\mathbf{x}}\hat{\mathbf{x}} : \nabla\mathbf{G}_{(3)}(\mathbf{x}) = \frac{\sigma}{8\pi\mu}\hat{\mathbf{x}}\hat{\mathbf{x}} : \nabla\mathbf{G}_{(3)}(\mathbf{x}). \tag{3}$$

For a given organism geometry and propulsive mechanism we therefore have a link between the swimming speed V_0 and the dipole strength σ with units of work, which in this case is $\sigma \approx 6\pi\mu A V_0 d$. Note that if $d \to 0$, for there to be a finite dipole value σ the force on the fluid from the cell body F_A must grow like $1/d$, which is possible so long as the instantaneous relative flagellum speed v increases as $1/d$ (though a more accurate treatment requires inclusion of hydrodynamic interactions). In general a swimming body induces higher moments in a multipole expansion [4]. Stresslet coefficients for ellipsoidal Janus particles are given in Refs. [4, 5]. Coarse-graining using the model above leads to the active stress written in the main paper. Experiments by Drescher et al. [1, 6] determined that the velocity field far from an *E. coli* cell was well approximated as a force dipole with strength $\sigma/(8\pi\mu) = -31.8\mu m^3/s$. Using a cell body size $\ell \approx 3\mu m$ and swimming speed $V_0 \approx 22\,\mu\,m/s$, for *E. coli* we have a dimensionless dipole strength $\alpha \approx -4(\ell/\ell_c)^2$, where ℓ_c is the mean free path (see the main text).

B. The flow due to a cylindrical, Gaussian colony of aligned particles

With $\Psi(\mathbf{x}, \mathbf{p}, t)$ the distribution of particles per volume in phase space (see the main text), the flow field generated by a single particle located at the origin in three-dimensions and pointing in a direction $\mathbf{p}_0$ is provided in the limiting case of $\Psi(\mathbf{x}, \mathbf{p}) = \tilde{\kappa}\delta_0(x)\delta_0(y)\delta_0(z)\delta_{\mathbf{p}_0}(\mathbf{p})$, where $\tilde{\kappa} = V/\ell_c^3$, ℓ_c is the characteristic particle size, and V is the volume of the spatial domain D. The delta functions are defined such that $\int_D \delta_{\mathbf{0}}(\mathbf{x})\,d\mathbf{x} = 1$ and $\int_S \delta_{\mathbf{p_0}}(\mathbf{p})\,d\mathbf{p} = 1$, where S is the unit ball ($|\mathbf{p}| = 1$).

Meanwhile, the flow field generated by a concentrated line of particles in the $\hat{\mathbf{z}}$ direction, centered at the origin in the xy-plane and all pointing in a direction $\mathbf{p}_0$, is instead provided by $\Psi(\mathbf{x}, \mathbf{p}) = \kappa\delta_0(x)\delta_0(y)\delta_{\mathbf{p}_0}(\mathbf{p})$. In this two-dimensional setting we require $\int_{\theta_0-\pi}^{\theta_0+\pi} \delta_{\theta_0}(\theta)\,d\theta = 1$, and we assume that motion is confined to the xy-plane. It is now more convenient to adjust the notation from vectors in $\mathbb{R}^3$ to vectors in $\mathbb{R}^2$, e.g. $\mathbf{x} = (x, y)$, $\mathbf{x}_0 = (x_0, y_0)$, $\mathbf{p} = (\cos\theta, \sin\theta)$, and $\mathbf{I}$ is the 2x2

identity matrix.

A useful approximation of the singular representation above is a cylindrical concentration which is Gaussian in its cross-sectional profile,

$$\Psi(x,y,\theta) = \frac{\kappa}{\pi^{3/2}a^2\varepsilon q(\varepsilon)} e^{-r^2/a^2-(\theta-\theta_0)^2/\varepsilon^2}, \tag{4}$$

with $r = \sqrt{x^2+y^2}$ and $\varepsilon \ll 1$, and $q(\varepsilon) = \mathrm{erf}(\pi/\varepsilon)$, which tends to 1 rapidly as $\varepsilon \to 0$, and κ is a normalization constant defined such that the total integral of Ψ is unity. The active stress on the fluid is then, for small ε,

$$\mathbf{\Sigma}_a(\mathbf{x}) = \alpha \int_{\theta_0-\pi}^{\theta_0+\pi} \Psi(x,y,\theta)\mathbf{p}\mathbf{p}\, d\theta = \frac{\alpha\kappa}{\pi a^2} e^{-r^2/a^2}\mathbf{p}_0\mathbf{p}_0 + O(\varepsilon^2), \tag{5}$$

where $\mathbf{\Sigma}_a$ is now represented as a 2x2 matrix. Part of the active stress only serves to modify the pressure and has no effect on the flow; it is common to extract this part by removing an isotropic tensor from $\mathbf{\Sigma}_a$, and to write

$$\mathbf{\Sigma}_a(\mathbf{x}) = \frac{\alpha\kappa}{\pi a^2} e^{-r^2/a^2}\left(\mathbf{p}_0\mathbf{p}_0 - \frac{1}{2}\mathbf{I}\right) + O(\varepsilon^2). \tag{6}$$

The body force on the fluid is then given by

$$\mathbf{f}_a = \nabla\cdot\mathbf{\Sigma}_a(\mathbf{x}) = -\frac{2\alpha\kappa}{\pi a^4} e^{-r^2/a^2}\left(\mathbf{p}_0(\mathbf{p}_0\cdot\mathbf{x}) - \frac{1}{2}\mathbf{x}\right). \tag{7}$$

Recalling that the system has been made dimensionless, with force density scaled upon $\mu V_0/\ell_c^2$ (μ is the viscosity, V_0 the dimensional swimming speed, and ℓ_c the mean free path), the pressure q and flow $\mathbf{u}$ which satisfy

$$-\nabla q + \nabla^2\mathbf{u} + \mathbf{f}_a = \mathbf{0}, \tag{8}$$

$$\nabla\cdot\mathbf{u} = 0, \tag{9}$$

and which are also independent of z are given by superposition,

$$\mathbf{u}(\mathbf{x}_0) = \frac{1}{4\pi}\int_{\mathbb{R}^2} \mathbf{G}(\mathbf{x_0}-\mathbf{x})\cdot\mathbf{f}_a(\mathbf{x})\, d\mathbf{x}, \tag{10}$$

$$\mathbf{G}(\mathbf{x}) = -\log(|\mathbf{x}|)\mathbf{I} + \frac{\mathbf{x}\mathbf{x}}{|\mathbf{x}|^2}, \tag{11}$$

where in this setting it is the two-dimensional Stokeslet singularity, $\mathbf{G}$, which arises [3].

To investigate the flow far from the origin we expand the Stokeslet singularity around $\mathbf{x} = \mathbf{0}$

and develop a multipole expansion,

$$\begin{aligned}\mathbf{u}(\mathbf{x}_0) &= \frac{1}{4\pi}\int_{\mathbb{R}^2} \mathbf{G}(\mathbf{x}_0)\cdot\mathbf{f}_a(\mathbf{x}) + [\mathbf{x}\cdot\nabla_{\mathbf{x}}\mathbf{G}(\mathbf{x}_0)]\cdot\mathbf{f}_a(\mathbf{x}) + [\frac{1}{2}\mathbf{x}\mathbf{x}:\nabla_{\mathbf{x}}\nabla_{\mathbf{x}}\mathbf{G}(\mathbf{x}_0)]\cdot\mathbf{f}_a(\mathbf{x}) + ...\, d\mathbf{x} \\ &= \frac{1}{4\pi}\mathbf{G}(\mathbf{x}_0)\cdot\int_{\mathbb{R}^2}\mathbf{f}_a(\mathbf{x})\,d\mathbf{x} + \frac{1}{4\pi}\nabla_{\mathbf{x}}\mathbf{G}(\mathbf{x}_0)\cdot\int_{\mathbb{R}^2}\mathbf{x}\mathbf{f}_a(\mathbf{x})\,d\mathbf{x} \\ &\quad + \frac{1}{8\pi}\nabla_{\mathbf{x}}\nabla_{\mathbf{x}}\mathbf{G}(\mathbf{x}_0):\int_{\mathbb{R}^2}\mathbf{x}\mathbf{x}\mathbf{f}_a(\mathbf{x}) + ...\, d\mathbf{x}, \end{aligned} \tag{12}$$

or in component form using Einstein summation notation,

$$u_i(\mathbf{x}_0) = \frac{1}{4\pi}G_{ij}(\mathbf{x}_0)F_j + \frac{1}{4\pi}\frac{\partial G_{ij}}{\partial x_k}(\mathbf{x}_0)S_{jk} + \frac{1}{8\pi}\frac{\partial^2 G_{ij}}{\partial x_k\partial x_m}(\mathbf{x}_0)R_{jkm} + ..., \tag{13}$$

where

$$F_j = \int_{\mathbb{R}^2} f_a(\mathbf{x})_j\,d\mathbf{x}, \quad S_{jk} = \int_{\mathbb{R}^2} x_k f_a(\mathbf{x})_j\,d\mathbf{x}, \quad R_{jkm} = \int_{\mathbb{R}^2} x_k x_m f_a(\mathbf{x})_j\,d\mathbf{x}. \tag{14}$$

Note that (taking care to distinguish the target point and derivative variable, $\mathbf{x}$, with the source point $\mathbf{x}_0$),

$$\begin{aligned}\frac{\partial G_{ij}}{\partial x_k}(\mathbf{x}_0) &= \frac{(x_0)_k\delta_{ij}}{|\mathbf{x}_0|^2} - \frac{\delta_{ik}(x_0)_j + \delta_{jk}(x_0)_i}{|\mathbf{x}_0|^2} + \frac{2(x_0)_i(x_0)_j(x_0)_k}{|\mathbf{x}_0|^4} \\ &= \frac{((x_0)_k\delta_{ij} - \delta_{ik}(x_0)_j - \delta_{jk}(x_0)_i)\,|\mathbf{x}_0|^2 + 2(x_0)_i(x_0)_j(x_0)_k}{|\mathbf{x}_0|^4}. \end{aligned} \tag{15}$$

Inserting the smoothed distribution into the expressions above we find $F_j = 0$ and $R_{jkm} = 0$ by symmetry, but

$$S_{jk} = \int_{\mathbb{R}^2} x_k f_a(\mathbf{x})_j\,d\mathbf{x} = -\alpha\kappa\left(\mathbf{p_0}\mathbf{p_0} - \frac{1}{2}\mathbf{I}\right)_{jk}, \tag{16}$$

and higher order terms with an odd number of derivatives in the series will also be non-zero. In the far-field, the velocity field is therefore a stresslet with

$$\mathbf{u}(\mathbf{x}_0) = \frac{-\alpha\kappa\mathbf{x}_0}{4\pi|\mathbf{x}_0|^2}\left(-1 + \frac{2(\mathbf{p}_0\cdot\mathbf{x}_0)^2}{|\mathbf{x}_0|^2}\right). \tag{17}$$

The identity part of the coefficient matrix $\mathbf{S}$ results in zero velocity contribution and only adjusts the local pressure. With $\mathbf{p}_0 = \hat{\mathbf{x}}$ we have, for $|\mathbf{x}_0| \gg 1$ and $\varepsilon \to 0$,

$$\mathbf{u}(\mathbf{x}_0) = \frac{-\alpha\kappa(x_0^2 - y_0^2)}{4\pi|\mathbf{x}_0|^4}\mathbf{x}_0. \tag{18}$$

For small $|\mathbf{x}_0|$, however, we have (in the limit as $\varepsilon \to 0$),

$$\mathbf{u}(\mathbf{x}_0) = \frac{\alpha\kappa(-x_0, y_0)}{8\pi a^2} + O(|\mathbf{x}_0|^2). \tag{19}$$

C. Connection of the Gaussian colony flow to regularized Stokeslets

There is a direct connection between the flow due to a cylindrical colony (or circular in two-dimensions) which is Gaussian in cross-section, and the flow due to a "regularized Stokeslet" [7]. In two-dimensions, the point force "blob" with small parameter $\tilde{\varepsilon}$,

$$\mathbf{f} = \frac{3\alpha\kappa\tilde{\varepsilon}^3}{2\pi(|\mathbf{x}_0|^2+\tilde{\varepsilon}^2)^{5/2}}\mathbf{p}, \tag{20}$$

results in the velocity field (see Ref. [7]):

$$\mathbf{u}^0(\mathbf{x}_0) = \frac{1}{4\pi}\left\{\left[-\log(\sqrt{|\mathbf{x}_0|^2+\tilde{\varepsilon}^2}+\tilde{\varepsilon}) + \frac{\tilde{\varepsilon}(\sqrt{|\mathbf{x}_0|^2+\tilde{\varepsilon}^2}+2\tilde{\varepsilon})}{(\sqrt{|\mathbf{x}_0|^2+\tilde{\varepsilon}^2}+\tilde{\varepsilon})\sqrt{|\mathbf{x}_0|^2+\tilde{\varepsilon}^2}}\right]\mathbf{I} + \frac{(\sqrt{|\mathbf{x}_0|^2+\tilde{\varepsilon}^2}+2\tilde{\varepsilon})}{(\sqrt{|\mathbf{x}_0|^2+\tilde{\varepsilon}^2}+\tilde{\varepsilon})^2\sqrt{|\mathbf{x}_0|^2+\tilde{\varepsilon}^2}}\mathbf{x_0}\mathbf{x_0}\right\}\cdot\mathbf{f}. \tag{21}$$

A derivative in the $\mathbf{p}$ direction gives the regularized force dipole,

$$\mathbf{u}(\mathbf{x}_0) = \mathbf{p}\cdot\nabla_{\mathbf{x}_0}\mathbf{u}^0(\mathbf{x}_0), \tag{22}$$

which is the same far-field flow as that described in the previous section. Looking in the near field we find that the association is precise when $\tilde{\varepsilon} = a\sqrt{3/2}$, where a is the Gaussian width of the cylindrical colony with Gaussian cross-section.

D. Self-stretching of aligned Gaussian colonies

As a preliminary step we first consider a circular Gaussian colony of nearly aligned particles,

$$\Psi(\mathbf{x},\theta,t=0) = Ce^{-r^2/a^2-\theta^2/\varepsilon^2}, \tag{23}$$

where $r = \sqrt{x^2+y^2}$, C is a numerically-determined normalization constant, and the periodic domain size $(x,y)\in[0,L)\times[0,H)$ is large enough to make negligible any effects from periodic spatial boundary conditions ($L = H = 50$ in the simulations). For motile pusher particles with Gaussian radius $a = 4$, angular spread $\varepsilon = 0.2$, and dipole strength $\alpha = -0.5$, numerical simulations reveal a nearly fore-aft symmetric self-stretching in the direction of motion (see the figure in the main text). Perturbing the initial data slightly by setting $r = \sqrt{x^2+(y-0.1\sin(2\pi x/L))^2}$ in (23), the dynamics are roughly unchanged for small times, but after the colony becomes sufficiently thin it undergoes a transverse concentration instability. Fore-aft symmetry is broken partly by the initial angular spread but primarily due to particle motility; the colony splays at the leading tip on the right, while undergoing a periodic folding at the rear reminiscent of the buckling of planar viscous jets, sedimenting elastic filaments, and beams extruded into viscous fluids.

A puller colony ($\alpha = 0.5$) instead elongates perpendicular to the swimming direction (also

shown in the main text), the perturbation appearing never to play a role, and a colony-scale splaying develops on the time-scale associated with the individual swimming speed. Videos of expanding pusher and puller colonies are included as Supplemental Material Movie M1.

To understand the dynamics of the initially polarized Gaussian patches we turn to equations describing the zeroth-moment of Ψ. Defining

$$c(\mathbf{x},t) = \langle 1 \rangle, \quad \mathbf{n}(\mathbf{x},t) = \frac{1}{c(\mathbf{x},t)} \langle \mathbf{p} \rangle, \tag{24}$$

$$\langle h(\mathbf{p}) \rangle = \int_{\Omega} h(\mathbf{p}) \psi(\mathbf{x},\mathbf{p},t)\, d\mathbf{p}, \tag{25}$$

and integrating the Smoluchowski equation we find

$$c_t + \nabla \cdot [(\mathbf{u} + V_0 \mathbf{n})c] = d_t \nabla^2 c. \tag{26}$$

In the locally aligned setting we have $\mathbf{n} \approx \mathbf{p_0}$, where $\mathbf{p_0}$ is the direction of alignment, and we study instead

$$c_t + \nabla \cdot [(\mathbf{u} + V_0 \mathbf{p_0})c] = d_t \nabla^2 c, \tag{27}$$

where V_0 is either 1 or 0 (motile or immotile). With $\mathbf{n} = \mathbf{p}_0$ fixed, and assuming that $c(\mathbf{x},t)$ remains in the shape of a Gaussian for all time, then the aspect ratio of a colony can be deduced if we are able to provide the velocity field $\mathbf{u}$ generated by the self-straining motion of the suspension. With the initially Gaussian colony defined in (4) with spatial radius a but with center of mass $\mathbf{x}_c(t) = (x_c(t), y_c(t))$ (taking $\mathbf{x}_c(0) = \mathbf{0}$) we have

$$\mathbf{u}(\mathbf{x}_0) = \frac{\alpha\kappa}{8\pi a^2} \left\{ -(x_0 - x_c), (y_0 - y_c) \right\}, \tag{28}$$

where

$$\mathbf{x}_c(t) = \frac{1}{\kappa} \int_{\mathbb{R}^2} \{x, y\} c(\mathbf{x},t)\, d\mathbf{x}, \tag{29}$$

which is normalized using $\kappa^{-1} \int_{\mathbb{R}^2} c(\mathbf{x},t)\, d\mathbf{x} = 1$. Importantly, we also make the approximation that $a(t) = b(t) = a_0$ in the velocity profile for all time, an approximation to which we will shortly return.

The axis lengths of the initially circular patch should vary as follows at small times. First we define the axis lengths $\{a(t), b(t)\}$ by the second spatial moment of the concentration about its center,

$$\{a(t)^2, b(t)^2\} = \frac{2}{\kappa} \int_{\mathbb{R}^2} \{(x - x_c(t))^2, (y - y_c(t))^2\} c(\mathbf{x},t)\, d\mathbf{x}. \tag{30}$$

For example if $c(\mathbf{x},t) = \kappa(\pi ab)^{-1} \exp(-[(x-x_c)^2/a^2 + (y-y_c)^2/b^2])$ this returns the values $a(t) = a$ and $b(t) = b$.

With $\mathbf{n} \approx \hat{\mathbf{x}}$ and inserting $\mathbf{u}$ from above, we have

$$c_t + V_0 c_x - \frac{\alpha\kappa}{8\pi a_0^2}((x - x_c(t))c_x - (y - y_c(t))c_y) = d_t \nabla^2 c. \tag{31}$$

If we assume that the concentration remains Gaussian over time, then

$$c(\mathbf{x}, t) = \frac{\kappa}{\pi a(t) b(t)} \exp\left(-\frac{(x - x_c(t))^2}{a(t)^2} - \frac{(y - y_c(t))^2}{b(t)^2}\right). \tag{32}$$

Given the symmetries inherent in this Gaussian profile, integration by parts reveals that

$$\frac{d}{dt}\mathbf{x}_c = \frac{1}{\kappa}\int_{\mathbb{R}^2} \{x, y\} c_t \, d\mathbf{x} = V_0 \hat{\mathbf{x}}. \tag{33}$$

A similar calculation leads to the dynamics of the semi-major and semi-minor axis lengths of the ellipsoidal patch,

$$\begin{aligned} \frac{d}{dt}\{a(t)^2, b(t)^2\} &= \{2a(t)a'(t), 2b(t)b'(t)\} \\ = \frac{2}{\kappa}\int_{\mathbb{R}^2} -2\{(x - x_c(t))x_c'(t), (y - y_c(t))y_c'(t)\} c(\mathbf{x}, t) &+ \{(x - x_c(t))^2, (y - y_c(t))^2\} c_t(\mathbf{x}, t) \, d\mathbf{x}, \end{aligned} \tag{34}$$

and integrating by parts we find

$$\{2a(t)a'(t), 2b(t)b'(t)\} = \left\{-\frac{\alpha\kappa a(t)^2}{4\pi a_0^2} + 4d_t, \frac{\alpha\kappa b(t)^2}{4\pi a_0^2} + 4d_t\right\}. \tag{35}$$

From this we deduce that

$$a(t) = \frac{a_0}{\sqrt{\alpha\kappa}}\sqrt{e^{-\frac{\alpha\kappa t}{4\pi a_0^2}}\left(\alpha\kappa + 16\pi d_t e^{\frac{\alpha\kappa t}{4\pi a_0^2}} - 16\pi d_t\right)}, \tag{36}$$

$$b(t) = \frac{a_0}{\sqrt{\alpha\kappa}}\sqrt{16\pi d_t e^{\frac{\alpha\kappa t}{4\pi a_0^2}} + \alpha\kappa e^{\frac{\alpha\kappa t}{4\pi a_0^2}} - 16\pi d_t}, \tag{37}$$

and hence an aspect ratio

$$r(t) = \frac{b(t)}{a(t)} = \frac{\sqrt{(\alpha\kappa + 16\pi d_t)e^{\alpha\kappa t/(4\pi a_0^2)} - 16\pi d_t}}{\sqrt{(\alpha\kappa - 16\pi d_t)e^{-\alpha\kappa t/(4\pi a_0^2)} + 16\pi d_t}}. \tag{38}$$

If $d_t = 0$ we have the simple result $r(t) = \exp[\alpha\kappa t/(4\pi a_0^2)]$ indicating a timescale for development of $\tau = 4\pi a_0^2/(|\alpha|\kappa)$. Taylor expanding $a(t)$ and $b(t)$ about $t = 0$ we find the approximation

$$r(t) = 1 + \frac{2\alpha\kappa t}{8\pi a_0^2 + (16\pi d_t - \alpha\kappa)t} + O(t^2). \tag{39}$$

Here we see a competition between diffusion, which seeks to return the aspect ratio to unity, and self-stretching, the direction of which depending on the sign of α: pushers ($\alpha < 0$) elongate in the

$\hat{\mathbf{x}}$ direction ($r(t)$ decreases from 1), pullers ($\alpha > 0$) elongate in the $\hat{\mathbf{y}}$ direction ($r(t)$ increases from 1).

Figure 3 shows the steadily decreasing aspect ratio of a colony of aligned pushers with $\alpha = -1$, with Gaussian initial concentration width $a_0 = 10$. The evolution is captured very well by fixing $\mathbf{n} = \hat{\mathbf{x}}$ and using the velocity field found numerically at $t = 0$, $\mathbf{u}(\mathbf{x}, t) = \mathbf{u}(\mathbf{x}, t = 0)$ (solid line in Fig. 3). The linear expansion of the velocity field around the origin results in the expression Eq. (38) and is shown as a dashed line. A cubic approximation to the velocity field, which results in a more accurate prediction (to be described), is shown as a dash-dotted line.

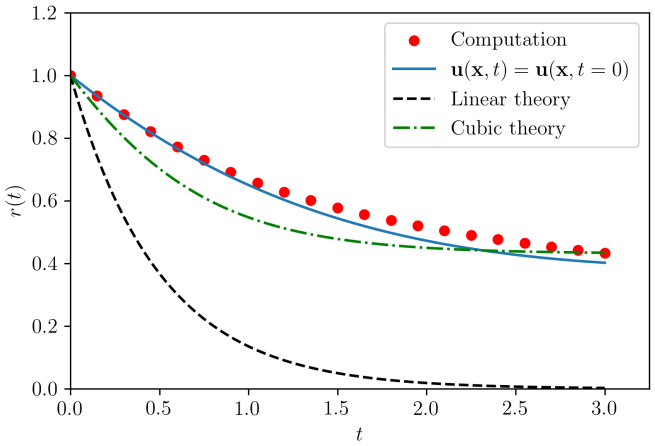

FIG. 3. The colony aspect ratio from simulations and different theoretical approximations. Solid line: fixing $\mathbf{n} = \hat{\mathbf{x}}$ and using the velocity field found numerically at $t = 0$, $\mathbf{u}(\mathbf{x}, t) = \mathbf{u}(\mathbf{x}, t = 0)$. Dashed line: prediction using the linearized velocity field near the origin, Eq. (38). Dash-dotted line: prediction using the cubic approximation of the velocity field near the origin, from Eq. (47).

The linear theory above captures the timescale for stretching but is not particularly accurate. While the velocity field in Eq. (19) used to derive Eq. (38) describes the stretching of a circular region smaller than the Gaussian width near the origin, it does not provide an accurate picture of the flow throughout the entire Gaussian colony; the leading order approximation of the velocity field becomes inaccurate at a distance from the origin smaller than the Gaussian width. Figure 4 shows the computed velocity field at $t = 0$ generated by a Gaussian colony of radius $a_0 = b_0 = 2$ and centered at $\mathbf{x}_c = (25, 25)$. The horizontal velocity along the cross-section at $y = 25$ is plotted as well, along with the far-field approximation from (18), the near-field linear approximation from (19), and a near-field cubic approximation (to be described). The departure of the linear approximation from the full velocity field becomes significant well before $|x - 25| = 2$.

A. Higher-order Taylor expansions of u

A cubic estimate of the velocity field, also shown along the central cross-section in Fig. 4, does improve the prediction of the aspect ratio, $r(t)$. The estimate up to $O(|\mathbf{x}|^4)$ (for a colony centered

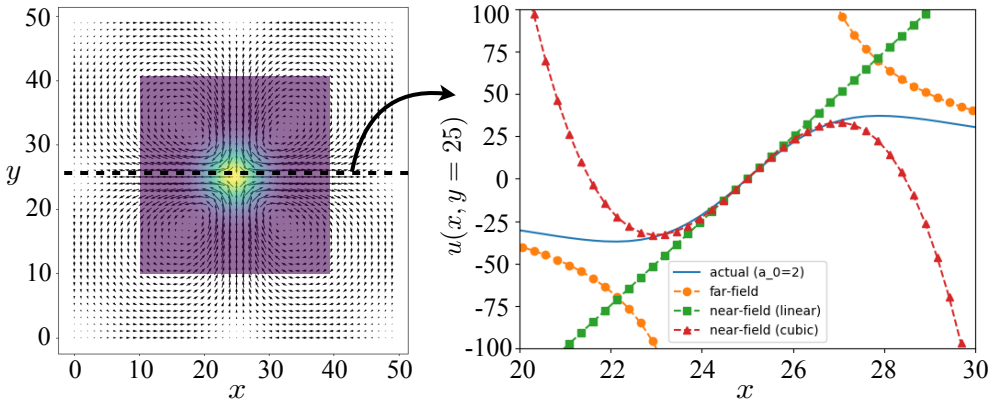

FIG. 4. Left: Velocity field at $t = 0$ due to a Gaussian colony of radius $a_0 = b_0 = 2$ placed at $(x_c, y_c) = (25, 25)$. Right: Numerical and competing approximations of the horizontal velocity along the cross-section at $y = 25$, from Eqs. (18), (19), and (40).

at the origin) is given by

$$\mathbf{u} = \frac{\alpha\kappa}{48\pi a^6}\left\{x\left(-6a^4 + 2a^2\left(x^2+3y^2\right) - 3x^2y^2\right), y\left(6a^4 - 2a^2\left(3x^2+y^2\right) + 3x^2y^2\right)\right\} + O(|\mathbf{x}|^4). \tag{40}$$

Integration as before results in the following:

$$a' = \frac{\alpha\kappa}{32\pi a_0^6}a^2\left(4a_0^2a^2\left(r^2+1\right) - 3a^4r^2 - 8a_0^4\right) + 4d_t, \tag{41}$$

$$b' = \frac{\alpha\kappa}{32\pi a_0^6}b^2\left(a^2\left(3b^2 - 4a_0^2\right) + 8a_0^4 - 4a_0^2b^2\right) + 4d_t, \tag{42}$$

and, if desired,

$$r' = \frac{\alpha\kappa}{32\pi a_0^6}a^2\left(4a_0^2a^2\left(r^2+1\right) - 3a^4r^2 - 8a_0^4\right) + \frac{4d_t}{a}. \tag{43}$$

Consider the case $d_t = 0$. Then $r'(t)/a'(t) = -2r(t)/a(t)$, so

$$r(t) = \frac{a_0^2}{a(t)^2}. \tag{44}$$

Inserting this into the equation for $a(t)$ we have

$$a'(t) = \frac{\alpha\kappa\left(-11a_0^2a(t)^2 + 4a(t)^4 + 4a_0^4\right)}{64\pi a_0^4 a(t)}. \tag{45}$$

Solving,

$$a(t) = a_0 \frac{\sqrt{\left(11 - \sqrt{57}\tanh\left(\frac{\sqrt{57}\alpha\kappa t}{64\pi a_0^2} + \tanh^{-1}\left(\sqrt{\frac{3}{19}}\right)\right)\right)}}{2\sqrt{2}}, \tag{46}$$

and thus

$$r(t) = \frac{8}{11 - \sqrt{57}\tanh\left(\frac{\sqrt{57}\alpha\kappa t}{64\pi a_0^2} + \tanh^{-1}\left(\sqrt{\frac{3}{19}}\right)\right)}. \tag{47}$$

For small t,

$$r(t) = 1 + \frac{3\alpha\kappa t}{32\pi a_0^2} + O(t^2). \tag{48}$$

E. Dynamics of an active sheet

We first examine the behavior of an infinite sheet of particles which are initially in near alignment. Figure 5 shows the evolution of a distribution of pusher particles with $\alpha = -1$, initially confined to a thin band and with a small transverse perturbation. Early stages show rapid growth of the wave amplitude. At the same time the vorticity field rotates individual particles so that they remain nearly tangent to the concentration band (see Supplemental Material Movie M2). What follows is a transient passage from one seemingly stationary attracting state to another until the system is finally drawn to the aperiodic roiling state described by Saintillan & Shelley [8]. The dynamics suggest the presence of numerous unstable stationary or periodic solutions.

To understand the initial instability we consider a line density of swimming particles and develop a theory to describe its evolution through far-field hydrodynamic self-interactions without translational or rotational diffusion. We identify the curve (a cross-section of an infinite two-dimensional sheet) as the zero level set of the function $F(x, y, t) = h(x, t) - y$, where $h(x, t)$ represents the curve's vertical displacement and $\phi(x, t)$ is the angle of the swimmer at station x relative to the x-axis. The evolution of F in the presence of the fluid velocity field $\mathbf{u} = (u, v)$ depends on the total velocity $\mathbf{u} + V_0\mathbf{p} = (u + V_0\cos\phi, v + V_0\sin\phi)$ (with $V_0 = 1$ for motile particles and $V_0 = 0$ for immotile particles) by

$$\frac{\partial h}{\partial t} + (u + V_0\cos\phi)\frac{\partial h}{\partial x} - (v + V_0\sin\phi) = 0, \tag{49}$$

which on the surface of the sheet, $y = h(x, t)$, is given by

$$\frac{\partial h}{\partial t} + (u + V_0\cos\phi)\,\frac{\partial h}{\partial x} - (v + V_0\sin\phi) = 0. \tag{50}$$

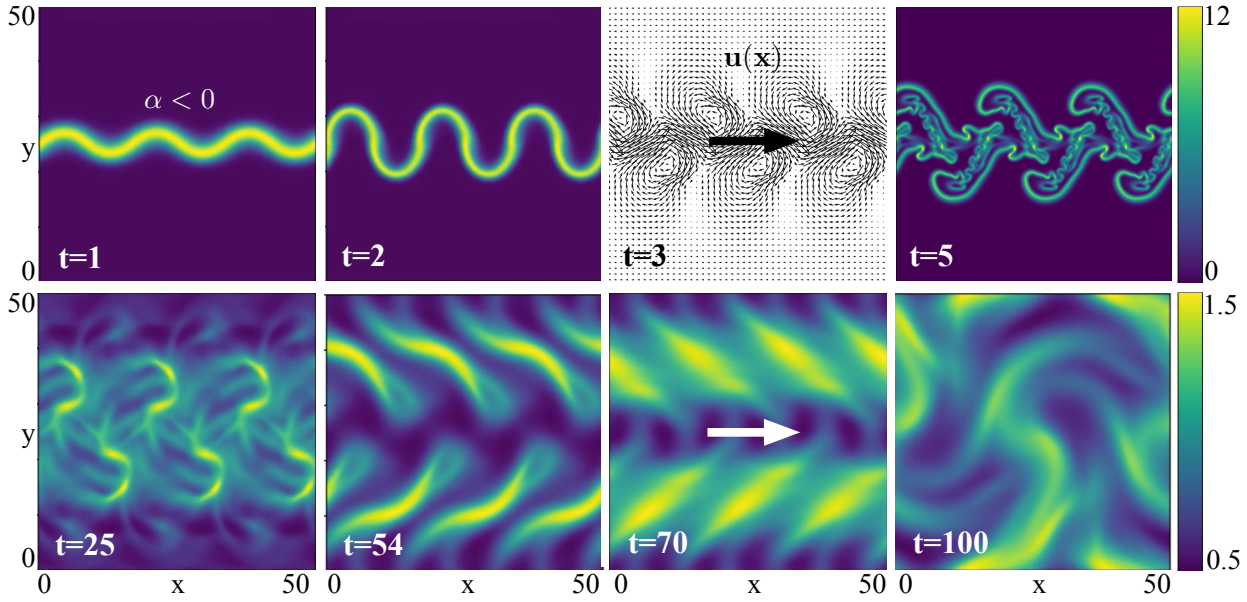

FIG. 5. Evolution of a thin band of motile pusher particles, $\alpha = -1$, with initial distribution function $\Psi(\mathbf{x}, \theta, t = 0) = C \exp\{-(y - \varepsilon\, h(x))^2/a^2 - \theta^2/b^2\}$ with C a normalization constant. The initial perturbation is given by $\varepsilon\, h(x) = 0.1 \sin(6\pi x/L)$ and $(a, b) = (2, 0.2)$. Exponential growth in amplitude leads to the development of an internal thrust-wake ($t = 3$) and a buckling cascade to smaller and smaller wavelengths ($t \in [3, 6]$). After passing through numerous almost stationary states, including looped ($t = 54$) and rotating aster ($t = 70$) patterns, symmetry is eventually broken and the suspension arrives in an aperiodic roiling state ($t = 100$). See Supplemental Material Movie M2.

For a nearly-flat surface (small h) we expand $\mathbf{u}(x, y, t)$ about $y = 0$ to find

$$\frac{\partial h}{\partial t} + \left(u|_{y=0} + h \frac{\partial u}{\partial y}\Big|_{y=0} + O(h^2) + V_0 \cos\phi \right) \frac{\partial h}{\partial x} - \left(v|_{y=0} + h \frac{\partial v}{\partial y}\Big|_{y=0} + O(h^2) + V_0 \sin\phi \right) = 0. \tag{51}$$

Meanwhile the swimming angle $\phi(x, t)$ in the Lagrangian frame evolves via

$$\frac{d\phi}{dt} = -u_x \sin(2\phi) + \frac{v_x}{2}(1 + \cos(2\phi)) - \frac{u_y}{2}(1 - \cos(2\phi)), \tag{52}$$

with subscripts indicating derivatives, so in the Eulerian frame we instead have

$$\frac{\partial \phi}{\partial t} + (u + V_0^* \cos\phi)\phi_x = -u_x \sin(2\phi) + \frac{v_x}{2}(1 + \cos(2\phi)) - \frac{u_y}{2}(1 - \cos(2\phi)). \tag{53}$$

Expanding also about $y = 0$ and $\phi = 0$ we have

$$\begin{aligned} &\frac{\partial \phi}{\partial t} + (u|_{y=0} + h\, u_y|_{y=0} + O(h^2) + V_0(1 + O(\phi^2)))\phi_x \\ &= -\left(u_x|_{y=0} + h\, u_{xy}|_{y=0} + O(h^2)\right)(2\phi + O(\phi^3)) + \frac{1}{2}\left(v_x|_{y=0} + h\, v_{xy}|_{y=0} + O(h^2)\right)(2 + O(\phi^2)) \\ &\qquad - \frac{1}{2}\left(u_y|_{y=0} + h\, u_{yy}|_{y=0} + O(h^2)\right)(O(\phi^2)). \end{aligned} \tag{54}$$

We now introduce the series expansions of h, ϕ and $\mathbf{u}$ as

$$h(x,t) = \varepsilon h^{(1)}(x,t) + \varepsilon^2 h^{(2)}(x,t) + O(\varepsilon^3), \tag{55}$$

$$\phi(x,t) = \varepsilon \phi^{(1)}(x,t) + \varepsilon^2 \phi^{(2)}(x,t) + O(\varepsilon^3), \tag{56}$$

$$\mathbf{u}(x,y,t) = \varepsilon \mathbf{u}^{(1)}(x,y,t) + \varepsilon^2 \mathbf{u}^{(2)}(x,y,t) + O(\varepsilon^3). \tag{57}$$

Up to order ε, we have

$$\frac{\partial h^{(1)}(x,t)}{\partial t} + V_0 \frac{\partial h^{(1)}(x,t)}{\partial x} = v^{(1)}(x,0,t) + V_0 \phi^{(1)}, \tag{58}$$

$$\frac{\partial \phi^{(1)}(x,t)}{\partial t} + V_0 \frac{\partial \phi^{(1)}(x,t)}{\partial x} = v_x^{(1)}(x,0,t). \tag{59}$$

Now, let us consider the influence of the line distribution on the velocity field. The following assumes an ansatz for the distribution:

$$\Psi(\mathbf{x},\theta,t) = \frac{\kappa}{\pi a b q(b) L} e^{-(y-\varepsilon h(x,t))^2/a^2 - [\theta - \varepsilon\phi(x,t)]^2/b^2}, \tag{60}$$

where $a/H \ll 1$, $b \ll 1$, and $\varepsilon \ll 1$, and $q(b) = \operatorname{erf}(\pi/b) \to 1$ rapidly as $b \to 0$ (recall the periodic domain is given by $(x,y) \in [0,L) \times [0,H)$, with $L = H = 50$ in the simulations, and then $\kappa = LH = 50^2$). Here $y = \varepsilon h(x,0)$ is the initial curve through space occupied by the active suspension (with small band thickness $a \ll 1$) and $\varepsilon\phi(x,0)$ is the initial particle orientation along that curve (tightly confined for $b \ll 1$). Note that for all time we have

$$\frac{1}{\kappa} \int_{x=0}^{L} \int_{y=-\infty}^{\infty} \int_{\theta=\varepsilon\phi-\pi}^{\varepsilon\phi+\pi} \Psi(\mathbf{x},\theta,t)\, d\theta\, dy\, dx = 1. \tag{61}$$

The associated fluid stress is

$$\begin{aligned} \boldsymbol{\Sigma}_a(\mathbf{x}) &= \alpha \int_{\varepsilon\phi-\pi}^{\varepsilon\phi+\pi} \Psi(\mathbf{x},\theta,t) \left(\mathbf{p}(x)\mathbf{p}(x) - \frac{1}{2}\mathbf{I} \right) d\theta \\ &= \frac{\alpha\kappa}{\pi^{1/2} a L} e^{-(y-\varepsilon h(x,t))^2/a^2} \left(\mathbf{p}_0(x)\mathbf{p}_0(x) - \frac{1}{2}\mathbf{I} \right) + O(\varepsilon^2, b^2), \end{aligned} \tag{62}$$

where $\mathbf{p}_0 = \hat{\mathbf{x}} + \varepsilon\phi(x,t)\hat{\mathbf{y}}$. Locally at a station x, this corresponds to a vertically integrated stress

$$\boldsymbol{\Sigma}_a(x) = \int_{y=-\infty}^{\infty} \boldsymbol{\Sigma}_a(\mathbf{x})\, dy = \frac{\alpha\kappa}{L} \left(\mathbf{p}_0(x)\mathbf{p}_0(x) - \frac{1}{2}\mathbf{I} \right) + O(\varepsilon^2). \tag{63}$$

Then the velocity at a point on the filament $\mathbf{x}_0 = (x, \varepsilon h(x,t))$ is given by the integrated effect

of the distribution of stresslets,

$$\begin{aligned}\mathbf{u}(x) &= \frac{1}{4\pi}\int_{\mathbb{R}^2} G_{ij}(\mathbf{x}-\mathbf{x}')f_j(\mathbf{x}')\,d\mathbf{x}' = \frac{1}{4\pi}\int_{\mathbb{R}^2} G_{ij}(\mathbf{x}-\mathbf{x}')\partial_k(\mathbf{\Sigma}_a)_{kj}(\mathbf{x}')\,d\mathbf{x}' \\ &= -\frac{1}{4\pi}\int_{\mathbb{R}^2} \partial_k G_{ij}(\mathbf{x}-\mathbf{x}')(\mathbf{\Sigma}_a)_{kj}(\mathbf{x}')\,d\mathbf{x}' \\ &= \frac{-\alpha\kappa}{4\pi L}\int_0^L \left\{\frac{1}{(x-x')}\hat{\mathbf{x}} + \varepsilon\frac{h(x,t)-h(x',t)}{(x-x')^2}\hat{\mathbf{y}}\right\} dx' + O(\varepsilon^2), \end{aligned} \tag{64}$$

where $\mathbf{G}(\mathbf{x}) = -\log(|\mathbf{x}|)\mathbf{I} + \mathbf{x}\mathbf{x}/|\mathbf{x}|^2$ as before. The orientation field $\phi(x,t)$ does not appear in the flow field up to first order in ε. The integrals above are to be taken in the principal value sense.

To continue the analysis we will assume periodicity in x, or alternatively for a finite patch to assume that $L \gg 1$ and that x is near the center of the domain and not near the endpoints, resulting first in the vanishing of the $\hat{\mathbf{x}}$ component of the velocity field. To investigate the $\hat{\mathbf{y}}$ component we expand $h(x,t)$ and $\phi(x,t)$ in a Fourier basis in space, writing

$$h(x,t) = \sum_k \hat{h}_k(t)e^{iqx}, \quad \phi(x,t) = \sum_k \hat{\phi}_k(t)e^{iqx}, \tag{65}$$

with $q = 2\pi k/L$. Then with $\xi = x' - x$,

$$\begin{aligned}\int_0^L \frac{h(x,t)-h(x',t)}{(x-x')^2}\,dx' &\approx \int_{-\infty}^{\infty} \frac{h(x,t)-h(x',t)}{(x-x')^2}\,dx' \\ &= \lim_{a\to 0}\int_{-\infty}^{-a} + \int_a^{\infty} \frac{h(x,t)-h(x+\xi,t)}{\xi^2}\,d\xi, \end{aligned} \tag{66}$$

resulting in

$$\mathbf{u}(x,t) = \frac{-\pi\varepsilon\alpha\kappa}{2L^2}\sum_k |k|\hat{h}_k(t)\exp(2\pi ikx/L)\hat{\mathbf{y}}, \tag{67}$$

and we also need $\partial\mathbf{u}/\partial x$, which is given by

$$\mathbf{u}_x(x) = \frac{-\pi^2 i\varepsilon\alpha\kappa}{L^3}\sum_k |k|\hat{h}_k(t)\exp(2\pi ikx/L)\hat{\mathbf{y}}. \tag{68}$$

Upon insertion into (58), we find

$$\hat{h}_k' + \frac{2\pi ikV_0}{L}\hat{h}_k = \frac{-\pi\alpha\kappa|k|}{2L^2}\hat{h}_k + V_0\hat{\phi}_k, \tag{69}$$

$$\hat{\phi}_k' + \frac{2\pi ikV_0}{L}\hat{\phi}_k = \frac{-\pi^2 ik|k|\alpha\kappa}{L^3}\hat{h}_k. \tag{70}$$

The solution of this system is given by

$$\begin{pmatrix}\hat{h}_k(t)\\ \hat{\phi}_k(t)\end{pmatrix} = \mathbf{P}\begin{pmatrix}e^{\lambda_+ t} & 0\\ 0 & e^{\lambda_- t}\end{pmatrix}\mathbf{P}^{-1}\begin{pmatrix}\hat{h}_k(0)\\ \hat{\phi}_k(0)\end{pmatrix}, \tag{71}$$

with eigenvalues given by

$$\lambda_\pm = \frac{\pi(-\alpha\kappa\,|k| - 8ikLV_0 \pm \gamma_k)}{4L^2}, \tag{72}$$

where $\gamma_k = \sqrt{\alpha\kappa(\alpha\kappa k^2 - 16iLV_0 k|k|)}$, and the associated eigenvectors (the columns of $\mathbf{P}$) are

$$\mathbf{p}_+ = \begin{pmatrix} \dfrac{iL\,(-\alpha\kappa|k| + \gamma_k)}{4\pi\alpha\kappa k|k|} \\ 1 \end{pmatrix}, \quad \mathbf{p}_- = \begin{pmatrix} \dfrac{iL\,(-\alpha\kappa|k| - \gamma_k)}{4\pi\alpha\kappa k|k|} \\ 1 \end{pmatrix}. \tag{73}$$

If the particles are not stress-generating, $\alpha = 0$, with $h(x, t = 0) = h_0(x)$ and $\phi(x, t = 0) = \theta_0^{(1)}(x)$, we find

$$\phi(x,t) = \phi_0(x - V_0 t), \tag{74}$$

$$h(x,t) = h(x - V_0 t) + t\,V_0 \phi(x - V_0 t), \tag{75}$$

so the wave amplitude grows linearly in time, just as expected, since any particles with nonzero initial angle simply drift off into space without resistance along characteristic curves.

In the other limit, we assume either immotile particles, $V_0 = 0$, or take the limit $|\alpha|/V_0 \to \infty$. Then if $\alpha > 0$ (pullers) we find $\lambda_+ = 0$ and $\lambda_- = -\pi\kappa|\alpha k|/(2L^2)$, with associated eigenvectors

$$\mathbf{p}_+ = \hat{\mathbf{y}}, \quad \mathbf{p}_- = -i\hat{\mathbf{x}} + \frac{2\pi k}{L}\hat{\mathbf{y}}. \tag{76}$$

Meanwhile, if $\alpha < 0$ (pushers) we find $\lambda_+ = \pi\kappa|\alpha k|/(2L^2)$ and $\lambda_- = 0$, with

$$\mathbf{p}_+ = -i\hat{\mathbf{x}} + \frac{2\pi k}{L}\hat{\mathbf{y}}, \quad \mathbf{p}_- = \hat{\mathbf{y}}. \tag{77}$$

Both include a neutral direction associated with a pure shift of the sheet in the vertical direction.

To measure the growth rates λ_+ and λ_- numerically the simulation is seeded with an initial condition given by (61), and we choose $h(x, t = 0) = \hat{h}_k(0)e^{iqx}$ and $\phi(x, t = 0) = \hat{\phi}_k(0)e^{iqx}$ with $q = 2\pi k/L$ such that the vector $[\hat{h}_k(0), \hat{\phi}_k(0)]$ is pointing in the direction of either eigenvector $\mathbf{p}_+$ or $\mathbf{p}_-$. The Smoluchowski equation is then evolved by a single time step with size $dt = 10^{-7}$. We designate $h(x,t)$ to be the center of mass location at each value of x in the y direction; in other words, we calculate $h(x,t) = \int yc(x,y,t)dy / \int c(x,y,t)dy$. In addition, we calculate ϕ by $\phi(x,t) = \arctan(\tilde{n}_y(x,t)/\tilde{n}_x(x,t))$ where $\tilde{n}_x(x,t) = \int n_x c(x,y,t)dy / \int c(x,y,t)dy$ and $\tilde{n}_y(x,t) = \int n_y c(x,y,t)dy / \int c(x,y,t)dy$. Then $\hat{h}_k$ and $\hat{\phi}_k$ are determined using a one dimensional Fourier transform of h and ϕ respectively. Finally, the growth rate is found by evaluating $\lambda_+ = \log\left(|\hat{\phi}_k(dt)|/|\hat{\phi}_k(0)|\right)/dt$. The results of this numerical investigation are shown in the main text, where we find a close agreement between the theory and the simulations.

F. Connection to the Kelvin-Helmholtz/Saffman-Taylor/Rayleigh-Taylor instabilities

The instability of a flat vortex sheet in an inviscid, inertial flow to sinusoidal perturbation is known as the Kelvin-Helmholtz instability. If the position of the two-dimensional sheet is parameterized by s and expressed in complex form, $z(s) = x(s) + iy(s)$, then the dynamics of the sheet are governed by the Birkhoff equation:

$$\frac{\partial z^*}{\partial t}(s,t) = \frac{1}{2\pi i}\fint_{-\infty}^{\infty} \frac{\gamma(s',t)}{z(s,t) - z(s',t)}\, ds', \tag{78}$$

where $z^*(s) = x(s) - iy(s)$, and $\gamma(s',t)$ is the vortex sheet strength, which moves with the flow, $\gamma_t(s,t) = 0$. Consider the simplest case, such that the vortex sheet strength is constant, $\gamma = \Gamma$. For a small sinusoidal perturbation we have the Ansatz $z(s,t) = s + i\varepsilon h(s,t)$, with $\varepsilon \ll 1$, so that

$$\frac{\partial z^*}{\partial t} = -i\varepsilon \frac{\partial h}{\partial t}(s,t) = \frac{\Gamma}{2\pi i}\fint_{-\infty}^{\infty} \frac{1}{(s-s') + i\varepsilon(h(s,t) - h(s',t))}\, ds'. \tag{79}$$

Expanding about $\varepsilon = 0$,

$$\frac{\partial h}{\partial t} = \frac{\Gamma}{2\pi}\fint_{-\infty}^{\infty} \frac{\varepsilon^{-1}}{s-s'} - i\frac{h(s,t) - h(s',t)}{(s-s')^2}\, ds', \tag{80}$$

and removing the singular part of the principle value integral, we find

$$\frac{\partial h}{\partial t} = \frac{-i\Gamma}{2\pi}\int_{-\infty}^{\infty} \frac{h(s,t) - h(s',t)}{(s-s')^2}\, ds', \tag{81}$$

which is precisely the form seen in (64) save for an extra factor of i, which acts to rotate the flow field by 90° in the complex plane.

Another view is offered by further consideration of the governing equations in (58), and we now make a connection between the first order velocity field and the Hilbert transform. Writing $\tilde{\alpha} = \alpha\kappa/(4L)$ (and suppressing the time dependence, for clarity) we have the vertical component of the velocity given by

$$\begin{aligned} v = -\frac{\tilde{\alpha}}{\pi}\int_0^L \frac{h(x) - h(x')}{(x-x')^2}\, dx' &\approx -\frac{\tilde{\alpha}}{\pi}\int_{-\infty}^{\infty} \frac{(h(x') + (x-x')h_x(x')) - h(x')}{(x-x')^2}\, dx' \\ &= -\frac{\tilde{\alpha}}{\pi}\int_{-\infty}^{\infty} \frac{h_x(x')}{x-x'}\, dx' = -\tilde{\alpha}\mathcal{H}[h_x], \end{aligned} \tag{82}$$

where

$$\mathcal{H}[f] = \frac{1}{\pi}\fint_{-\infty}^{\infty} \frac{f(x')}{x-x'}\, dx' \tag{83}$$

is the Hilbert transform. The operator $\mathcal{H}$ is skew-symmetric, commutes with differentiation for sufficiently smooth data (i.e. $\partial_x\mathcal{H}[f] = \mathcal{H}[f_x]$), and has trigonometric functions as eigenvectors

($\mathcal{H}[e^{iqx}] = -i\,\mathrm{sign}(q)e^{iqx}$). The principle system may therefore be written as

$$h_t + V_0 h_x = -\tilde{\alpha}\mathcal{H}[h_x] + V_0\phi, \tag{84}$$

$$\phi_t + V_0\phi_x = -\tilde{\alpha}\mathcal{H}[h_{xx}]. \tag{85}$$

Applying the operator $(\partial_t + V_0\partial_x)$ to the first equation and using the second we find

$$(\partial_t + V_0\partial_x)^2 h = -\tilde{\alpha}\mathcal{H}[h_{xt} + 2V_0 h_{xx}]. \tag{86}$$

In the immotile case, with $V_0 = 0$, the dynamics of h reduce to

$$h_t = -\tilde{\alpha}\mathcal{H}[h_x]. \tag{87}$$

This is the exact form found in the evolution of the interface between two fluids of the same viscosity but different density, either confined between two closely-spaced plates (in a Hele-Shaw cell) or in a two-dimensional porous medium flow, without surface tension, whose flow governed by Darcy's Law. With or without the viscosity difference and surface tension this is also known as the Muskat problem (see the main text for references).

G. Proof of the "no-flow theorem"

The proof assumes uniqueness of solutions to the full Smoluchowski - Stokes system described in the main text, which was shown for two-dimensions by Chen & Liu [9]. Suppose that Ψ is initially isotropic in orientation, $\Psi(\mathbf{x}, \mathbf{p}, t = 0) = \Psi_0(\mathbf{x})$, and consider the following modified system of equations:

$$\Psi_t + \nabla \cdot (\dot{\mathbf{x}}\Psi) + \nabla_{\mathbf{p}} \cdot (\dot{\mathbf{p}}\Psi) = 0, \tag{88}$$

$$\dot{\mathbf{x}} = V_0\mathbf{p} - d_t\nabla\left(\ln\Psi\right), \tag{89}$$

$$\dot{\mathbf{p}} = -d_r\nabla_{\mathbf{p}}\left(\ln\Psi\right), \tag{90}$$

$$-\nabla q + \nabla^2\mathbf{u} + \nabla\cdot\boldsymbol{\Sigma}_a = \mathbf{0}, \tag{91}$$

$$\nabla\cdot\mathbf{u} = 0, \tag{92}$$

$$\boldsymbol{\Sigma}_a(\mathbf{x}) = \sigma\int_\Omega \mathbf{p}\mathbf{p}^T\Psi(\mathbf{x},\mathbf{p},t)\,d\mathbf{p}, \tag{93}$$

where $\nabla = \nabla_{\mathbf{x}}$ and $\nabla_{\mathbf{p}} = (\mathbf{I} - \mathbf{pp})\cdot\partial/\partial\mathbf{p}$, and the spatial domain is either unbounded or periodic. Note that the terms coupling the time evolution of Ψ to the flow $\mathbf{u}$ have been removed from the original system of equations. Thus Ψ is determined completely by (88)-(90) and the provided initial condition Ψ_0. We will show that the velocity generated by $\Psi(\mathbf{x}, \mathbf{p}, t)$ is zero for all space and time when Ψ is initially isotropic in orientation. We will then demonstrate that this same Ψ solves the original system of equations.

From (91) and (92), the flow $\mathbf{u}$ in Fourier space is given by

$$\hat{\mathbf{u}} = \frac{1}{|\mathbf{k}|^2}(\mathbf{I} - \hat{\mathbf{k}}\hat{\mathbf{k}}) \cdot \hat{\mathbf{\Sigma}} \cdot \mathbf{k}. \tag{94}$$

Note that if $\hat{\mathbf{\Sigma}} \cdot \mathbf{k} = \lambda_{\mathbf{k}}(t)\mathbf{k}$ for some scalar function $\lambda_{\mathbf{k}}(t)$, then $\hat{\mathbf{u}} = \mathbf{0}$. We will demonstrate that this is in fact the case. Combining (88) – (90), we have that

$$\Psi_t + V_0\mathbf{p} \cdot \nabla_{\mathbf{x}}\Psi - d_t\nabla^2_{\mathbf{x}}\Psi - d_r\nabla^2_{\mathbf{p}}\Psi = 0. \tag{95}$$

Performing a spatial Fourier transform we find

$$\hat{\Psi}_t - iV_0\mathbf{p} \cdot \mathbf{k}\hat{\Psi} + d_t|\mathbf{k}|^2\hat{\Psi} - d_r\nabla^2_{\mathbf{p}}\hat{\Psi} = 0, \tag{96}$$

where $\hat{\Psi} = \hat{\Psi}_{\mathbf{k}}(\mathbf{p}, t)$. Note that (96) is non-autonomous in $\mathbf{p}$; this results in Fourier mode coupling if a Fourier decomposition is performed in $\mathbf{p}$ as well. Instead, we continue by making the transformations: $\hat{\mathbf{k}} = \boldsymbol{R} \cdot \hat{\mathbf{z}}$ and $\mathbf{p} = \mathbf{R} \cdot \mathbf{q}$ where $\mathbf{R}$ is a rotation matrix. Then (96) may be written as

$$\hat{\Psi}_t - iV_0|\mathbf{k}|\mathbf{q} \cdot \hat{\mathbf{z}}\hat{\Psi} + d_t|\mathbf{k}|^2\hat{\Psi} - d_r\nabla^2_{\mathbf{q}}\hat{\Psi} = 0, \tag{97}$$

where now $\hat{\Psi} = \hat{\Psi}_{\mathbf{k}}(\mathbf{q}, t)$.

We proceed to demonstrate that $\hat{\mathbf{\Sigma}} \cdot \mathbf{k} = \lambda_{\mathbf{k}}(t)\mathbf{k}$. This intermediate result is the primary part of the proof with dependency on dimensionality. Thus two- and three-dimensional analysis are now treated independently.

Two-dimensions: In two-dimensions we write $\mathbf{q}$ in terms of polar coordinates:

$$\hat{\Psi}_t - iV_0|\mathbf{k}|\cos\theta\hat{\Psi} + d_t|\mathbf{k}|^2\hat{\Psi} - d_r\nabla^2_{\mathbf{q}}\hat{\Psi} = 0, \tag{98}$$

where $\nabla^2_{\mathbf{q}} = \partial_{\theta\theta}$ and $\hat{\Psi} = \hat{\Psi}_{\mathbf{k}}(\theta, t)$. Since the *isotropic* initial condition and equations are invariant with respect to the transformation $\theta \to -\theta$, the solution is also invariant with respect to these transformations. Thus, $\hat{\Psi}_{\mathbf{k}}(\theta, t) = \hat{\Psi}_{\mathbf{k}}(-\theta, t)$. We now compute $\hat{\mathbf{\Sigma}} \cdot \mathbf{k}$:

$$\hat{\mathbf{\Sigma}} \cdot \mathbf{k} = \int_\Omega \mathbf{p}\mathbf{p} \cdot \mathbf{k}\hat{\Psi}_{\mathbf{k}}(\mathbf{p}, t)\, d\mathbf{p}. \tag{99}$$

Then applying the transform $\mathbf{p} = \boldsymbol{R} \cdot \mathbf{q}$, we find

$$\hat{\mathbf{\Sigma}} \cdot \mathbf{k} = |\mathbf{k}|\boldsymbol{R} \cdot \int_\Omega \mathbf{q}\mathbf{q} \cdot \hat{\mathbf{z}}\hat{\Psi}_{\mathbf{k}}(\mathbf{q}, t)\, d\mathbf{q}. \tag{100}$$

We now transform to variable θ:

$$\hat{\mathbf{\Sigma}} \cdot \mathbf{k} = |\mathbf{k}|\boldsymbol{R} \cdot \int_{-\pi}^{\pi} d\theta\, \mathbf{q}(\theta)\cos\theta\hat{\Psi}_{\mathbf{k}}(\theta, t), \tag{101}$$

where $\mathbf{q}(\theta) = (\sin\theta, \cos\theta)$. Given that Ψ is even with respect to θ, it follows that the $\hat{\mathbf{z}}$ component only remains in the integral. We are left with

$$\hat{\boldsymbol{\Sigma}} \cdot \mathbf{k} = |\mathbf{k}| \boldsymbol{R} \cdot \hat{\mathbf{z}} \int_{-\pi}^{\pi} d\theta \, \cos^2\theta \hat{\Psi}_{\mathbf{k}}(\theta, t), \tag{102}$$

which provides the desired result,

$$\hat{\boldsymbol{\Sigma}} \cdot \mathbf{k} = \lambda_{\mathbf{k}}(t)\mathbf{k}, \tag{103}$$

where

$$\lambda_{\mathbf{k}}(t) = \int_{-\pi}^{\pi} d\theta \, \cos^2\theta \hat{\Psi}_{\mathbf{k}}(\theta, t), \tag{104}$$

and finally $\hat{\mathbf{u}} = 0$.

Three-dimensions: In three-dimensions we instead write $\mathbf{q}$ in terms a spherical coordinate system,

$$\hat{\Psi}_t - iV_0|\mathbf{k}|\cos\theta\hat{\Psi} + d_t|\mathbf{k}|^2\hat{\Psi} - d_r\nabla_{\mathbf{q}}^2\hat{\Psi} = 0, \tag{105}$$

where $\nabla_{\mathbf{q}}^2 = (\sin\phi)^{-2}\partial_{\theta\theta} + (\sin\phi)^{-1}\partial_{\phi}\,(\sin\phi\,\partial_{\phi})$ and $\hat{\Psi} = \hat{\Psi}_{\mathbf{k}}(\theta, \phi, t)$. Since the initial condition and equations are invariant with respect to the transformations $\theta \to -\theta$ and $\phi \to -\phi$ independently, the solution is also invariant with respect to these transformations by uniqueness. Thus, $\hat{\Psi}_{\mathbf{k}}(\theta, \phi, t) = \hat{\Psi}_{\mathbf{k}}(-\theta, \phi, t)$ and $\hat{\Psi}_{\mathbf{k}}(\theta, \phi, t) = \hat{\Psi}_{\mathbf{k}}(\theta, -\phi, t)$. We now compute $\hat{\boldsymbol{\Sigma}} \cdot \mathbf{k}$:

$$\hat{\boldsymbol{\Sigma}} \cdot \mathbf{k} = \int_{\Omega} \mathbf{pp} \cdot \mathbf{k}\hat{\Psi}_{\mathbf{k}}(\mathbf{p}, t)\, d\mathbf{p}, \tag{106}$$

by applying the transform $\mathbf{p} = \boldsymbol{R} \cdot \mathbf{q}$:

$$\hat{\boldsymbol{\Sigma}} \cdot \mathbf{k} = |\mathbf{k}| \boldsymbol{R} \cdot \int_{\Omega} \mathbf{qq} \cdot \hat{\mathbf{z}}\hat{\Psi}_{\mathbf{k}}(\mathbf{q}, t)\, d\mathbf{q}. \tag{107}$$

Transforming to azimuthal and polar angles θ and ϕ, we have

$$\hat{\boldsymbol{\Sigma}} \cdot \mathbf{k} = |\mathbf{k}| \boldsymbol{R} \cdot \int_0^{\pi} d\theta \int_0^{2\pi} d\phi\, \mathbf{q}(\theta, \phi) \cos\theta \hat{\Psi}_{\mathbf{k}}(\theta, \phi, t), \tag{108}$$

where $\mathbf{q}(\theta, \phi) = (\sin\theta\cos\phi, \sin\theta\sin\phi, \cos\theta)$. Given that Ψ is even with respect to both θ and ϕ independently, it follows that only the $\hat{\mathbf{z}}$ component remains in the integral. We are left with

$$\hat{\boldsymbol{\Sigma}} \cdot \mathbf{k} = |\mathbf{k}| \boldsymbol{R} \cdot \hat{\mathbf{z}} \int_0^{\pi} d\theta \int_0^{2\pi} d\phi \, \cos^2\theta \hat{\Psi}_{\mathbf{k}}(\theta, \phi, t). \tag{109}$$

Therefore we find that

$$\hat{\boldsymbol{\Sigma}} \cdot \mathbf{k} = \lambda_{\mathbf{k}}(t)\mathbf{k}, \tag{110}$$

where

$$\lambda_{\mathbf{k}}(t) = \int_0^{\pi} d\theta \int_0^{2\pi} d\phi \, \cos^2\theta \hat{\Psi}_{\mathbf{k}}(\theta, \phi, t) \tag{111}$$

and finally $\hat{\mathbf{u}} = 0$.

Given that we have established that $\hat{\mathbf{\Sigma}} \cdot \mathbf{k} = \lambda_{\mathbf{k}}(t)\mathbf{k}$ for both two- and three-dimensions, and consequently that $\hat{\mathbf{u}} = 0$, we now observe that the distribution Ψ that solves the system (88)-(93) also solves the original system by the inclusion of the velocity terms (which are zero):

$$\Psi_t + \nabla_{\mathbf{x}} \cdot (\dot{\mathbf{x}}\Psi) + \nabla_{\mathbf{p}} \cdot (\dot{\mathbf{p}}\Psi) = 0, \tag{112}$$

$$\dot{\mathbf{x}} = V_0\mathbf{p} + \mathbf{u}(\mathbf{x}) - d_t\nabla_{\mathbf{x}} (\ln \Psi), \tag{113}$$

$$\dot{\mathbf{p}} = (\mathbf{I} - \mathbf{pp}) \cdot (\mathbf{p} \cdot \nabla\mathbf{u}) - d_r\nabla_{\mathbf{p}} (\ln \Psi), \tag{114}$$

$$-\nabla q + \nabla^2\mathbf{u} + \nabla \cdot \mathbf{\Sigma}_a = \mathbf{0}, \tag{115}$$

$$\nabla \cdot \mathbf{u} = 0, \tag{116}$$

$$\mathbf{\Sigma}_a(\mathbf{x}) = \sigma \int_{\Omega} \mathbf{pp}^T \Psi(\mathbf{x}, \mathbf{p}, t) \, d\mathbf{p}. \tag{117}$$

And assuming uniqueness of solutions to this system (see Ref. [9]), $\mathbf{u}$ is zero for any initial condition that is isotropic in orientation.

---

[1] K. Drescher, J. Dunkel, L.H. Cisneros, S. Ganguly, and R. E. Goldstein. Fluid dynamics and noise in bacterial cell–cell and cell–surface scattering. *Proc. Natl. Acad. Sci. USA*, 108:10940–10945, 2011.

[2] J. Dunkel, S. Heidenreich, K. Drescher, H. H. Wensink, M. Bär, and R. E. Goldstein. Fluid dynamics of bacterial turbulence. *Phys. Rev. Lett.*, 110:228102, 2013.

[3] C. Pozrikidis. *Boundary Integral and Singularity Methods for Linearized Viscous Flow.* Cambridge University Press, Cambridge, UK, 1992.

[4] S. E. Spagnolie and E. Lauga. Hydrodynamics of self-propulsion near a boundary: predictions and accuracy of far-field approximations. *J. Fluid Mech.*, 700:105–147, 2012.

[5] E. Lauga and S. Michelin. Stresslets induced by active swimmers. *Phys. Rev. Lett.*, 117:148001, 2016.

[6] K. Drescher, R. E. Goldstein, N. Michel, M. Polin, and I. Tuval. Direct measurement of the flow field around swimming microorganisms. *Phys. Rev. Lett.*, 105:168101, 2010.

[7] R. Cortez. The method of regularized Stokeslets. *SIAM J. Sci. Comput.*, 23(4):1204–1225, 2001.

[8] D. Saintillan and M. J. Shelley. Instabilities, pattern formation, and mixing in active suspensions. *Phys. Fluids*, 20:123304, 2008.

[9] X. Chen and J.-G. Liu. Global weak entropy solution to Doi–Saintillan–Shelley model for active and passive rod-like and ellipsoidal particle suspensions. *J. Differential Equations*, 254(7):2764–2802, 2013.